Reprinted from JOURNAL OF PHYSICAL OCEANOGRAPHY, Vol. 23, No. 8, August 1993
American Meteorological Society

Statistics of Shear and Turbulent Dissipation Profiles in Random Internal Wave Fields*

M. C. GREGG,** H. E. SEIM,** AND D. B. PERCIVAL†

Applied Physics Laboratory, College of Ocean and Fishery Sciences, University of Washington, Seattle, Washington

(Manuscript received 4 March 1992, in final form 2 November 1992)

ABSTRACT

Because breaking internal waves produces most of the turbulence in the thermocline, the statistics of ϵ, the rate of turbulent dissipation, cannot be understood apart from the statistics of internal wave shear. The statistics of ϵ and shear are compared for two sets of profiles from the northeast Pacific. One set, PATCHEX, has internal wave shear close to the Garrett and Munk model, but the other set, PATCHEX north, has average 10-m shear squared, $\langle S_{10}^2 \rangle$, about four times larger than the model.

The 10-m shear components, S_x and S_y, were measured between 1 and 9 MPa and referenced to a common stratification by WKB scaling. The scaled components, $\hat{S}_x$ and $\hat{S}_y$, are found to be independent and normally distributed with zero means, as assumed by Garrett and Munk. This readily leads to analytic forms for the probability densities of $\hat{S}_{10}^2$ and $\hat{S}_{10}^4$. The observed probability densities of $\hat{S}_{10}^2$ and $\hat{S}_{10}^4$ are close to the predicted forms, and both are strongly skewed. Moreover, $\sigma_{\ln \hat{S}_{10}^2}$ and $\sigma_{\ln \hat{S}_{10}^4}$ are constants, independent of the standard deviations of $\hat{S}_x$ and $\hat{S}_y$. The probability density of the inverse Richardson number, $\mathrm{Ri}_{10}^{-1} = S_{10}^2/\langle N^2 \rangle$, is a scaled version of the probability density of S_{10}^2. The PATCHEX distribution cuts off near $\mathrm{Ri}_{10}^{-1} = 4$, as found by Eriksen, but the PATCHEX north distribution extends to higher values, as predicted analytically. Consequently, a cutoff at $\mathrm{Ri}_{10}^{-1} = 4$ is not a universal constraint.

Over depths where $\langle N^2 \rangle$ is nearly uniform, the probability density of 0.5-m ϵ can be approximated, to varying degrees of accuracy, as the sum of a noise variate with an empirically determined distribution and a lognormally distributed variate whose parameters can be estimated using a minimum chi-square fitting procedure. The 0.5-m ϵ, however, are far from being uncorrelated, a circumstance not considered by Baker and Gibson in their analysis of microstructure statistics. Obtaining approximately uncorrelated samples requires averaging over 10 m for PATCHEX and 15 m for PATCHEX north. These lengths correspond approximately to reciprocals of the wavenumbers at which the respective shear spectra roll off. After correcting the uncorrelated ϵ samples for noise and then scaling to remove the dependence on stratification, the scaled dissipation rates, $\hat{\epsilon} = \epsilon(N_0^2/\langle N^2 \rangle)$, are lognormally distributed. (Without noise correction and $\langle N^2 \rangle$ scaling the data are not lognormal; e.g., noise correction and scaling with $\langle N^1 \rangle$ and $\langle N^{3/2} \rangle$ do not produce lognormality.)

It is hypothesized that the approximate lognormality of bulk ensembles of $\hat{\epsilon}$ results from generation of turbulence in proportion to $\hat{S}_{10}^4$. Lognormality is well established for isotropic homogeneous turbulence (Gurvich and Yaglom), and Yamazaki and Lueck show that it also occurs within individual turbulent patches. Bulk ensembles from the thermocline, however, include samples from many sections lacking turbulence as well as from a wide range of uncorrelated turbulent events at different evolutionary stages. Consequently, the bulk data do not meet the criteria used to demonstrate lognormality under more restricted conditions. If the authors are correct, the high-amplitude portion of $\langle N^2 \rangle$-scaled bulk ensembles is lognormal or nearly so owing to generation of the turbulence by a highly skewed shear moment. As another consequence, $\sigma_{\ln \hat{S}_{10}^4} = 2.57$ should be an upper bound for 10 m $\tilde{\sigma}_{\ln \hat{\epsilon}}$ when the turbulence is produced by the breaking of random internal waves. Because many parts of the profile lack turbulence, sensor noise limits the ϵ distribution to smaller spreads than those of $\hat{S}_{10}^4$. In practice we observe $\tilde{\sigma}_{\ln \hat{\epsilon}} \approx 1.2$ when $\hat{S}_{10}^2$ equals GM76, and $\tilde{\sigma}_{\ln \hat{\epsilon}} \approx 1.5$ when $\hat{S}_{10}^2$ is about three times GM76. For the larger spread, 95% confidence limits require $n \approx 60$ for accuracies of ±100%, $n \approx 140$ for ±50%, and $n \approx 2000$ for ±10%. Owing to instrumental uncertainties in ϵ estimates, the authors suggest accepting less restrictive confidence limits at one site and sampling at multiple sites to estimate average dissipation rates in the thermocline.

1. Introduction

For the past 20 years, attempts to estimate turbulence and vertical diffusivity in the thermocline have been statistical in nature, relying on bulk averages of microstructure parameters rather than on detailed time series of mixing events. At the same time, Garrett and Munk (1972a) parameterized the average characteristics of the background internal wave field in terms of the local buoyancy frequency, N. Garrett and Munk (1972b) then applied this parameterization to the rate at which internal waves randomly break. Munk (1981) and De-

* School of Oceanography, University of Washington, Contribution Number 1961.

** Other affiliation: School of Oceanography, University of Washington, Seattle, Washington.

† Other affiliation: Department of Statistics, University of Washington, Seattle, Washington.

Corresponding author address: Dr. M. C. Gregg, Applied Physics Laboratory, University of Washington, 1013 NE 40th St., Seattle, WA 98105-6698.

saubies and Smith (1982) refined these approaches, and McComas and Müller (1981) and Henyey et al. (1986) extended the analysis by showing that the rate at which interactions within the internal wave field move energy toward small scales and ultimate dissipation depends on N and E, the dimensionless energy density of the internal wave field. That is, $\epsilon_{iw} \propto \langle N^2 \rangle E^2$, where $\langle \quad \rangle$ denotes an arithmetic mean. If this line of development is correct, the average dissipation rate, $\langle \epsilon \rangle$, depends only on these average parameters and is thus independent of the physical mechanisms producing the dissipation.

Because free-fall profilers do not adequately measure E, which is dominated by very low wavenumbers, Gregg (1989) recasts the McComas and Müller (1981) and Henyey et al. (1986) results in terms of the variance of internal wave shear,

$$\epsilon_{iw} \equiv 7 \times 10^{-10} \frac{\langle N^2 \rangle}{N_0^2} \frac{S_{10}^4}{S_{GM}^4} \quad [\mathrm{W\ kg^{-1}}], \qquad (1)$$

where $N_0 = 0.0052\ \mathrm{s}^{-1}$, S_{10}^4 is the fourth moment of the 10-m shear produced by random internal waves, and S_{GM}^4 is the corresponding moment for the Garrett and Munk (1975) model. [This model is known as GM76 when modifications by Cairns and Williams (1976) are included.] The revised scaling was applied to six sets of profiles of instantaneous shear and dissipation from sites where internal waves provide most of the shear. For these data, the largest ratio of $\langle \epsilon \rangle / \nu \langle N^2 \rangle$ is 283 times the smallest (ν is the kinematic viscosity and $\langle \epsilon \rangle / \nu \langle N^2 \rangle$ is a measure of the intensity of turbulence in stratified fluids). Applying (1) reduces this range to a factor of 3. Therefore, in view of the limited variability of $\langle N^2 \rangle$ in the thermocline, variability in shear appears to be the principal factor causing variations in $\langle \epsilon \rangle$. Wavenumber spectra of this shear variability are given by Gregg et al. (1992).

To examine whether (1) applies to individual 10-m estimates, we use two sets of profiles taken with the multiscale profiler (MSP) between 1 and 9 MPa (100 to 900 m) during the Patches Experiment (PATCHEX) in the eastern North Pacific. The first dataset (Gregg and Sanford 1988) contains 27 profiles from a diffusively stable thermocline in which the variance of finescale shear is close to GM76. Several days after the main PATCHEX observations, five profiles, referred to as PATCHEX north, were taken below a week-old coastal jet off northern California. The shear variance of the second dataset is about four times GM76. Of the six datasets used by Gregg (1989) to compare ϵ and shear, only the two sets analyzed here, PATCHEX and PATCHEX north, contain simultaneous measurements of ϵ and shear with internal waves at average or above-average intensity.

To treat the observations in each dataset as single ensembles, the N dependence of the profiles is removed with

$$\hat{\epsilon}_{iw} = \epsilon_{iw} \left(\frac{N_0^2}{N^2} \right) \qquad (2)$$

and

$$\hat{\epsilon} = \epsilon \left(\frac{N_0^2}{N^2} \right). \qquad (3)$$

Thus, $\hat{\epsilon}_{iw}$ is a simple scaling of the fourth shear moment; that is, combining (1) and (2) yields

$$\hat{\epsilon}_{iw} = 0.959 S_{10}^4, \qquad (4)$$

where the constant has units of meters squared per second, and N scaling of shear is defined in the next section. In Fig. 1, $\hat{\epsilon}_{iw}$ is plotted on the x axes, and $\hat{\epsilon}$ is on the y axes. As is evident in the top panel, 10-m pairs are weakly correlated and have trends beginning near $\log_{10} \mathrm{Ri}_{10}^{-1} = 0$. Nevertheless, the large scatter demonstrates that equality between $\hat{\epsilon}$ and $\hat{\epsilon}_{iw}$ does not apply to individual estimates but to averages. Averaging over 100 m greatly reduces the scatter, and using 800 m produces a tight distribution about the dashed line representing the model.

Because (1) applies only to averages, we treat the scaling as a relation between two random processes. Specifically, we

- test how well our observations can be modeled by random processes,
- examine to what degree probability densities of $\hat{\epsilon}$ and $\hat{\epsilon}_{iw}$ are related,
- form confidence limits for these variables, and
- examine what the confidence limits imply about sampling.

Gargett (1990) suggests that scalings other than (1) provide equally good fits to data. This may be true, but, for the 100-m and 800-m averages plotted in Fig. 1, two-sample Kolmogoroff–Smirnoff tests show no significant differences between the $\hat{\epsilon}$ and $\hat{\epsilon}_{iw}$ distributions. Consequently, we cannot reject the hypothesis that in each case $\hat{\epsilon}$ and $\hat{\epsilon}_{iw}$ are identical populations. Therefore, whether or not (1) is a unique scaling, it adequately relates averages of dissipation and shear. Determining which scaling is best will require 1) additional simultaneous measurements of shear, N, and ϵ; and 2) careful examination of the statistics. We initiate the latter in this paper and focus on the averaging required to collapse widely scattered pairs of $\hat{\epsilon}$ and $\hat{\epsilon}_{iw}$ to the close equality found between their averages.

In section 2 the normality of the shear components is tested and probability densities are developed for S_{10}^2, Ri_{10}^{-1}, and S_{10}^4. After a brief review of the lognormality of ϵ at the beginning of section 3, we test the lognormality of our data and then compare the probability densities of $\hat{\epsilon}$ and $\hat{\epsilon}_{iw}$. In section 4 we present confidence limits for the shear moments and for lognormal ϵ data, and we also discuss implications for sampling. We conclude in section 5 with a summary

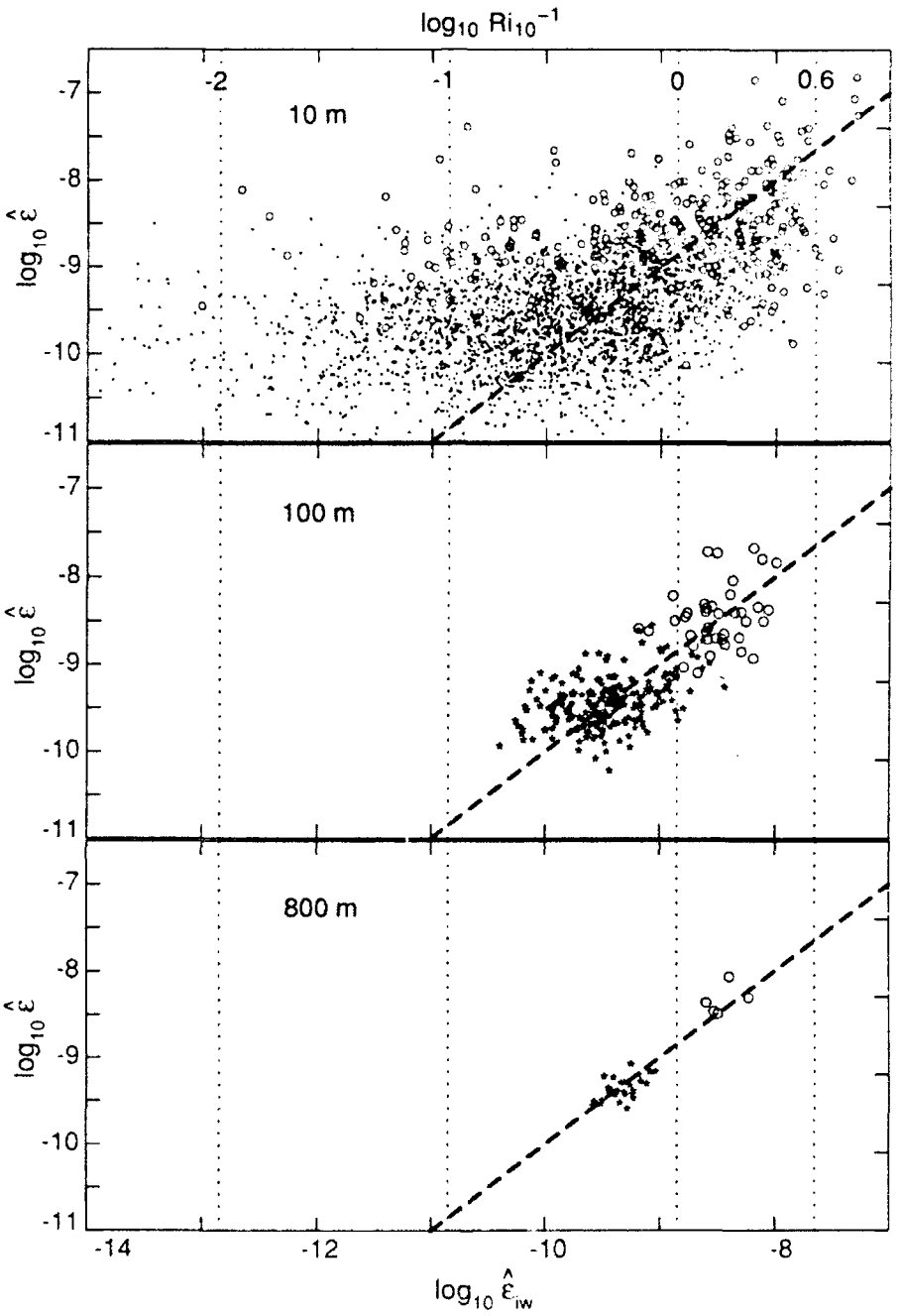

FIG. 1. Scatterplots of $\log_{10}\hat{\epsilon}$ versus $\log_{10}\hat{\epsilon}_{iw}$ for averages over 10 m, 100 m, and 800 m. PATCHEX data are shown by dots in the top panel and stars in the lower panels. PATCHEX north data are shown by open circles. The heavy dashed line is $\log_{10}\hat{\epsilon} = \log_{10}\hat{\epsilon}_{iw}$.

and discussion. Throughout the paper we use nonparametric statistical tests wherever possible. Often several tests are applied to examine different aspects of the data. To maintain continuity in the discussion while being thorough with the statistics, many details of the tests are in the appendixes.

2. Statistics of shear and its moments

Our goal in this section is to investigate how well instantaneous shear and its moments can be represented as random processes, as assumed by GM76. This involves first demonstrating uncorrelatedness, in the vertical and pairwise between components. Then we can form moments of the data and test whether the distributions fit analytic models. Because tests applied to individual profiles are not rigorous, owing to small sample sizes, we use several methods for each hypothesis we test, expecting gross departures from our hypotheses to be apparent in all tests. We note minor departures, but assume that their presence does not

invalidate further development. Details of statistical tests used in this section are in appendices A–C.

a. The shear components, $\hat{S}_x$ and $\hat{S}_y$

With eastward and northward flow represented by U and V, the shear components are computed as

$$S_x \equiv \sqrt{2.11}\left(\frac{\Delta U}{\Delta z}\right), \quad S_y \equiv \sqrt{2.11}\left(\frac{\Delta V}{\Delta z}\right), \tag{5}$$

with $\Delta z = 10$ m (Gregg and Sanford 1988). The factor of $\sqrt{2.11}$ corrects for the attenuation of the first-difference filter, making the shear variance comparable to an integral of GM76 to 0.6 rad m^{-1} (0.1 cycle per meter). Systematic changes resulting from changes in stratification are removed with

$$\hat{S}_x \equiv S_x\left(\frac{N_0}{\langle N^2\rangle^{1/2}}\right), \quad \hat{S}_y \equiv S_y\left(\frac{N_0}{\langle N^2\rangle^{1/2}}\right). \tag{6}$$

Based on two nonparametric statistical tests, the run test and the spectral distribution function, we cannot reject at the 5% level of significance the hypothesis that for PATCHEX $\hat{S}_x$ and $\hat{S}_y$ are vertically independent, although there is some evidence of weak vertical correlation. (See appendix A for details.) Neither can we reject the hypothesis that the shear components are pairwise independent of each other. We thus assume the PATCHEX shear components are independent both in the vertical and pairwise. This, however, is not true for PATCHEX north, as one of the five profiles is rejected by both tests (appendix A).

Means and standard deviations of N-scaled and unscaled shear components are given in Table 1. Although N scaling has little effect on the standard deviations for PATCHEX, it increases by 50% the standard deviations for PATCHEX north. Taking $\tilde{\sigma}_x$ and $\tilde{\sigma}_y$ as the sample standard deviations of $\hat{S}_x$ and $\hat{S}_y$, we compute normal probability densities having zero means and $\tilde{\sigma}_s \equiv (1/2)(\tilde{\sigma}_x + \tilde{\sigma}_y)$. (For PATCHEX $\tilde{\sigma}_s = 2.79 \times 10^{-3}$ s^{-1}, and for PATCHEX north $\tilde{\sigma}_s = 4.83 \times 10^{-3}$ s^{-1}.) As seen in the lower panels of Fig. 2, overlaying these normal probability densities and histograms of the observations reveals good fits.

TABLE 1. Means and standard deviations of 10-m shear components. The PATCHEX distributions have 2187 samples, and the PATCHEX north distributions have 405 samples. Parameters scaled with $\langle N^2\rangle$ are overstruck with a circumflex.

	Mean	Standard deviation
	PATCHEX	
S_x	-2.20×10^{-5}	2.50×10^{-3}
S_y	-4.26×10^{-5}	2.63×10^{-3}
$\hat{S}_x$	-4.88×10^{-5}	2.74×10^{-3}
$\hat{S}_y$	-3.68×10^{-5}	2.84×10^{-3}
	PATCHEX north	
S_x	-2.68×10^{-5}	3.33×10^{-3}
S_y	-5.79×10^{-6}	3.20×10^{-3}
$\hat{S}_x$	-7.25×10^{-5}	4.91×10^{-3}
$\hat{S}_y$	7.82×10^{-6}	4.74×10^{-3}

Working with our assumption of independence, we apply the Lilliefors test statistic (appendix A) to test the hypothesis that $\hat{S}_x$ and $\hat{S}_y$ are normally distributed with zero means and common variances. We find that, at the 5% level of significance, we cannot reject this hypothesis. A visual equivalent of this test is displayed in the upper panels of Fig. 2, which show quantile–quantile (q–q) plots (Chambers et al. 1983), with observed distributions along the vertical axes and fitted normal distributions along the horizontal axes. If the observed distributions were identical to the fitted distributions, the data would plot along diagonals from lower left to upper right. The Lilliefors test statistics provide a way of plotting 95% confidence limits to assess whether observed departures from the diagonal are consistent with random deviations. For both datasets, $\hat{S}_x$ remains within the 95% confidence limits, as is the case for $\hat{S}_y$ (not shown). Therefore, we can treat the shear components as normally distributed with zero means. Under this assumption, we use an F test to find that, at the 5% level of significance, the variances of $\hat{S}_x$ and $\hat{S}_y$ can be taken to be the same.

b. The second moment, $\hat{S}^2_{10}$, and the inverse Richardson number

Unscaled and scaled second moments are

$$S^2_{10} \equiv S^2_x + S^2_y, \quad S^2_{10} \equiv \hat{S}^2_x + \hat{S}^2_y. \tag{7}$$

When $\hat{S}_x$ and $\hat{S}_y$ are normally distributed and uncorrelated, the probability density of $\hat{S}^2_{10}$ can be calculated readily because it is the sum of the squares of $\hat{S}_x$ and $\hat{S}_y$. The result is an exponential distribution (Papoulis 1984),

$$P_y = \frac{\exp(-y/2\sigma_s^2)}{2\sigma_s^2} H(y), \text{ with } y = \hat{S}^2_{10} = \hat{S}^2_x + \hat{S}^2_y; \tag{8}$$

$H(y) = 1$ for $y \geq 0$ and $H(y) = 0$ for $y < 0$. (If normalized to $\sigma_s^2 = 1$, P_y is χ^2 with two degrees of freedom.) The q–q plots of $\log_{10}\hat{S}^2_{10}$ show the PATCHEX distribution slightly crossing the 95% confidence limits but all the PATCHEX north distribution remaining inside (Fig. 3). (The probability density of $\log_{10}\hat{S}^2_{10}$ is derived in appendix B.)

To the degree that the gradient Richardson number is not influenced by fluctuations in N^2 induced by internal waves, the probability density of $\log_{10}\mathrm{Ri}^{-1}_{10}$ is simply a shifted version of the probability density of the second moment of the scaled shear; that is, $\log_{10}\mathrm{Ri}^{-1}_{10} = \log_{10}\hat{S}^2_{10} + 4.57$, where $\log_{10}N_0^2 = -4.57$. The critical value for dynamic instability of parallel shear flows is $\mathrm{Ri}_c^{-1} = 4$ (Miles 1961), corresponding to $\log_{10}$

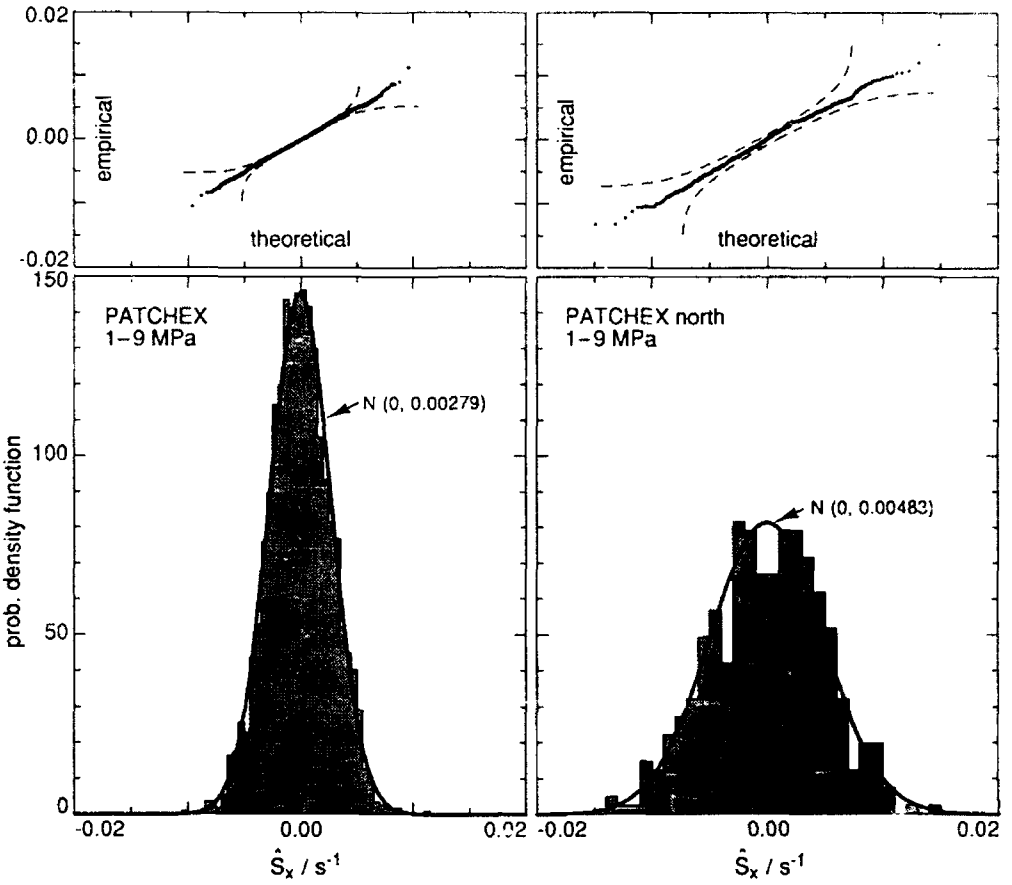

FIG. 2. In the lower panels, normal probability densities having zero means and standard deviations of σ_s are shown by heavy lines. The observed probability densities of $\hat{S}_x$ are shaded. In the upper panels, q-q plots have the observed (empirical) distributions along the vertical axes and the normal (theoretical) distributions along horizontal axes. The observed distributions fall within the 95% confidence limits of the theoretical distributions (dashed lines), which are much wider for PATCHEX north, 405 samples, than for PATCHEX, 2152 samples. Appendix A describes calculation of the 95% confidence limits.

$\mathrm{Ri}_c^{-1} = 0.6$. From the $\log_{10} \mathrm{Ri}_{10}^{-1}$ scale in Fig. 3, we see that the PATCHEX distribution drops to zero just to the left of 0.6, similar to previous reports of cutoffs of Richardson number at the critical value (Eriksen 1978, 1982). Only 0.2% of the PATCHEX samples have $\log_{10} \mathrm{Ri}_{10}^{-1} > 0.6$, compared with 17.5% exceeding $\log_{10} \mathrm{Ri}_{10}^{-1} > 0$. The observed probability density for PATCHEX north also follows the theoretical prediction, but it does not cut off at the critical value; 9% of the samples exceed $\log_{10} \mathrm{Ri}_{10}^{-1} = 0.6$, and 56% have $\log_{10} \mathrm{Ri}_{10}^{-1} > 0$. Replotting in more conventional form (Fig. 4) shows the PATCHEX north Richardson numbers peaking sharply between 0.25 and 0.5.

Munk (1981) argues that saturation of the shear spectrum prevents Richardson numbers from dropping below 1/4, even when the shear rises above the background state modeled in GM76. He bases his argument on observations by Eriksen (1978), who computed the Richardson number by first-differencing data from current meters moored 7 m apart in the vertical. Eriksen did not discuss the energy level of the internal waves, but review of his data shows that the energy level cannot be distinguished from GM76 (Eriksen 1991, personal communication). Thus, Eriksen's observations are fully consistent with our distribution for PATCHEX, but the PATCHEX north distribution demonstrates that Eriksen's result cannot be generalized; 10-m Richardson numbers smaller than one-fourth occur for shears above GM76.

c. *The fourth moment, $\hat{S}_{10}^4$*

Unscaled and N-scaled fourth moments are

$$S_{10}^4 \equiv (S_{10}^2)^2, \quad \hat{S}_{10}^4 \equiv (\hat{S}_{10}^2)^2. \tag{9}$$

As shown in appendix B, we can use (8) to obtain the probability density of $\hat{S}_{10}^4$; namely,

$$P_w = \frac{P_y(y_1)}{|g'(y_1)|} = \frac{\exp(-y/2\sigma_s^2)}{4y\sigma_s^2} H(y),$$

$$w = y^2 = \hat{S}_{10}^4. \tag{10}$$

Provided that $\hat{S}_x$ and $\hat{S}_y$ are normally distributed and uncorrelated, the standard deviation of the natural log-

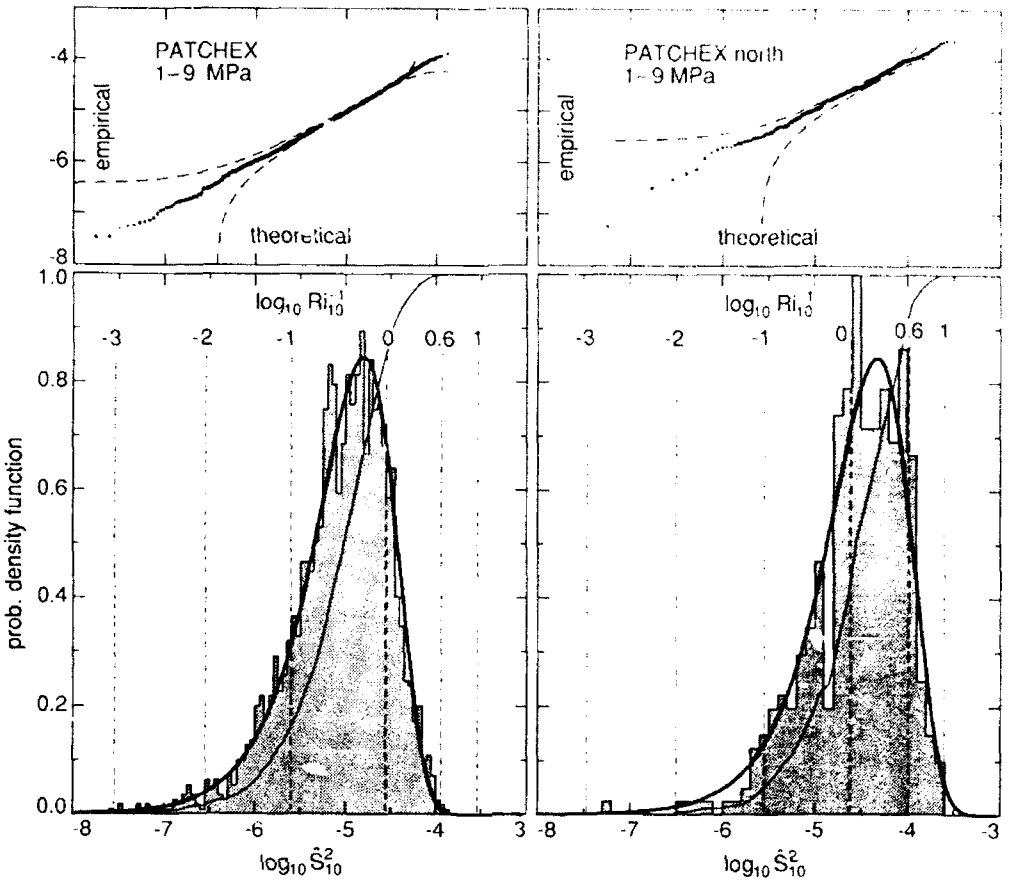

FIG. 3. In the lower panels, observed probability densities of $\log_{10}\hat{S}^2_{10}$ (shaded) are compared with the predicted form (B1), shown as heavy curves. The light curves are the cumulative distribution functions of the observed distributions. Vertical dotted lines mark constant values of $\log_{10} \mathrm{Ri}_{10}^{-1}$. The critical Richardson number of 0.25 corresponds to $\log_{10} \mathrm{Ri}_{10}^{-1} = 0.6$. In the upper panels, q–q plots have the observed (empirical) distributions along the vertical axes and the theoretical distributions along horizontal axes. Part of the PATCHEX distribution falls slightly outside the 95% confidence limits, but none of the PATCHEX north distribution exceeds the confidence limits. Confidence limits were computed using the exponential case of Mason and Bell (1986).

arithm of the $\hat{S}^4_{10}$, $\sigma_{\ln \hat{S}^4_{10}}$, is a constant equal to 2.57 and does not change with variations in E. The distribution of $\log_{10}\hat{S}^4_{10}$ (B11) is highly skewed, with a long tail extending to very small values. Comparison with the observed probability densities shows parts of the PATCHEX distribution slightly outside the 95% confidence limits on q–q plots and all of the PATCHEX north distribution inside the limits (Fig. 5).

To investigate why the PATCHEX distributions fall just outside the 95% confidence limits, we examined the vertical correlation structure of the shear moments. As discussed in appendix C, we find no evidence of vertical correlatedness in $\hat{S}^4_{10}$, but there are indications of temporal correlatedness. For PATCHEX, direct evidence comes from averaging $\hat{S}^2_{10}$ and $\hat{S}^4_{10}$ vertically over 100 m and applying run tests to time series in each pressure range. For both moments, two of the eight series fail the run test, although $\hat{S}_x$ and $\hat{S}_y$ pass. We are uncertain of the reason, but believe it likely that near-inertial motions dominate the shear. Owing to their rotation, they rapidly decorrelate $\hat{S}_x$ and $\hat{S}_y$ but not $\hat{S}^2_{10}$ and $\hat{S}^4_{10}$. In addition, when data from all profiles in the same cruise are treated in a single ensemble, the standard deviations of $\log_{10}\hat{S}^2_{10}$ and $\log_{10}\hat{S}^4_{10}$ do not decrease as rapidly as they should for independent samples (appendix C). In some cases, observed standard deviations exceed predictions by more than 50%. The discrepancies are largest when averages of full profiles are compared, which suggests weak temporal coherence.

d. Summary

Probability densities of $\hat{S}_x$ and $\hat{S}_y$ are adequately approximated with normal distributions having zero means and common variance. Empirical tests suggest that $\hat{S}_x$ and $\hat{S}_y$ are uncorrelated for PATCHEX, but PATCHEX north may have some correlatedness. Assuming uncorrelatedness, we derive analytic forms for the probability densities of $\log_{10}\hat{S}^2_{10}$ and $\log_{10}\hat{S}^4_{10}$. Ob-

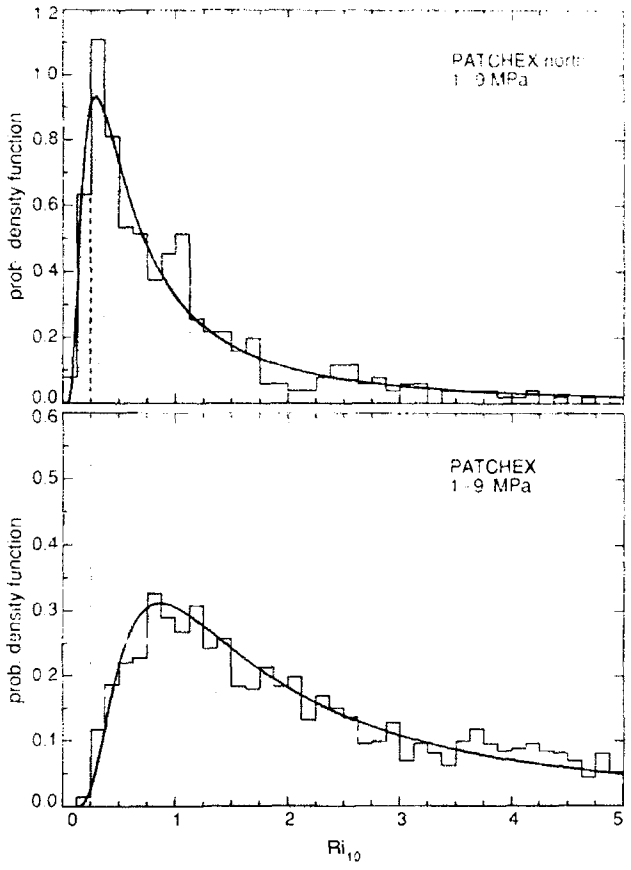

FIG. 4. Observed probability densities of Ri_{10} (shaded) compared with predicted forms (solid lines). At low values, both observed distributions cut off as predicted theoretically. For PATCHEX, the cutoff is close to $Ri_{10} = 1/4$. For PATCHEX north, the cutoff occurs at smaller values, and 9% of its samples are smaller than 1/4.

served probability densities of these moments are close to the predictions, with the PATCHEX north distribution within the 95% confidence limits and the PATCHEX distribution slightly outside at some places. Because this pattern is contrary to what would be expected from the correlation tests on $\tilde{S}_x$ and $\tilde{S}_y$, we suspect that the discrepancy results from weak temporal coherence between the PATCHEX profiles and that this coherence results from near-inertial motions. Probability densities of Richardson number, computed using the mean stratification, agree with the predicted distributions. The PATCHEX distribution cuts off near $Ri_{10} = 1/4$, as found by Eriksen (1978), but the PATCHEX north distribution extends to smaller values. Therefore, a cutoff at $Ri_{10} = 1/4$ is not a universal condition.

3. Statistics of dissipation

Turbulence is inherently intermittent. Even when turbulence is statistically homogeneous, local concentrations of small-scale shear determine average dissipation rates, $\langle \epsilon \rangle$, throughout the entire volume. Consequently, the sampling problem is to observe enough of the infrequent large values to ensure precise averages.

For statistically homogeneous and isotropic turbulent flows, Gurvich and Yaglom (1967) show that the turbulent cascade leads to lognormal probability densities of ϵ; that is, $\ln\epsilon$ is normally distributed. Lognormal distributions are typical for positive-definite variables produced by repeated multiplicative applications of a random process. For example, the sizes of sand grains broken off nearby rocks are lognormal, as are dissipation rates of the smallest eddies in a turbulent cascade. Lognormal probability densities are parameterized by $\mu_{\ln\epsilon}$ and $\sigma_{\ln\epsilon}$, the mean and standard deviation of $\ln\epsilon$. Gurvich and Yaglom (1967) argue that $\sigma_{\ln\epsilon}$, which measures intermittence, and hence the difficulty of sampling, increases with Reynolds number. At present, however, there is no way to estimate $\sigma_{\ln\epsilon}$ a priori, even in homogeneous turbulence (Yamazaki and Lueck 1990).

The airfoil probes used on MSP to detect velocity microstructure also respond to thermal transients having frequencies of 0.1–1 Hz (Osborn and Crawford 1980). At the MSP fall rate, these frequencies correspond to wavenumbers of 0.3–3 cpm. To minimize the effect of thermal transients and to detect short-length changes in turbulent intensity, we compute ϵ by integrating spectra taken over 0.5-m data windows.

In examining the statistics of ϵ, we must consider whether the samples are correlated. Only with uncorrelated samples can we accurately bound the degree of intermittence and estimate confidence limits for bulk ensembles of dissipation. Uncorrelatedness has not been addressed previously—investigators have merely assumed it, regardless of sample length or local circumstances. For example, Baker and Gibson (1987) assume uncorrelatedness for 0.23–1.15-m samples along horizontal tows taken by Washburn and Gibson (1984) and for 100–200-m samples along profiles taken by Gregg (1977). Confidence limits computed using standard deviations from positively correlated data are usually optimistic: that is, they give tighter limits than warranted.

a. Probability densities of 0.5-m ϵ

Probability histograms of $\log_{10}\epsilon$ for the 0.5-m samples are highly skewed, with long tails at large magnitudes and sharp cutoffs at low magnitudes (Fig. 6). Probability distributions have long been described as resulting from approximately lognormal oceanic signals at high magnitudes and noise at low magnitudes. Observations are considered noise when their spectral level drops to a low level that is only approximately constant because the ensembles are collected using probes having different noise levels and sensitivities. For MSP this level is 10^{-10} W kg^{-1} (Gregg and Sanford 1988). Because ϵ is positive definite, noise distributions are not expected to be normal but are closer to lognormal.

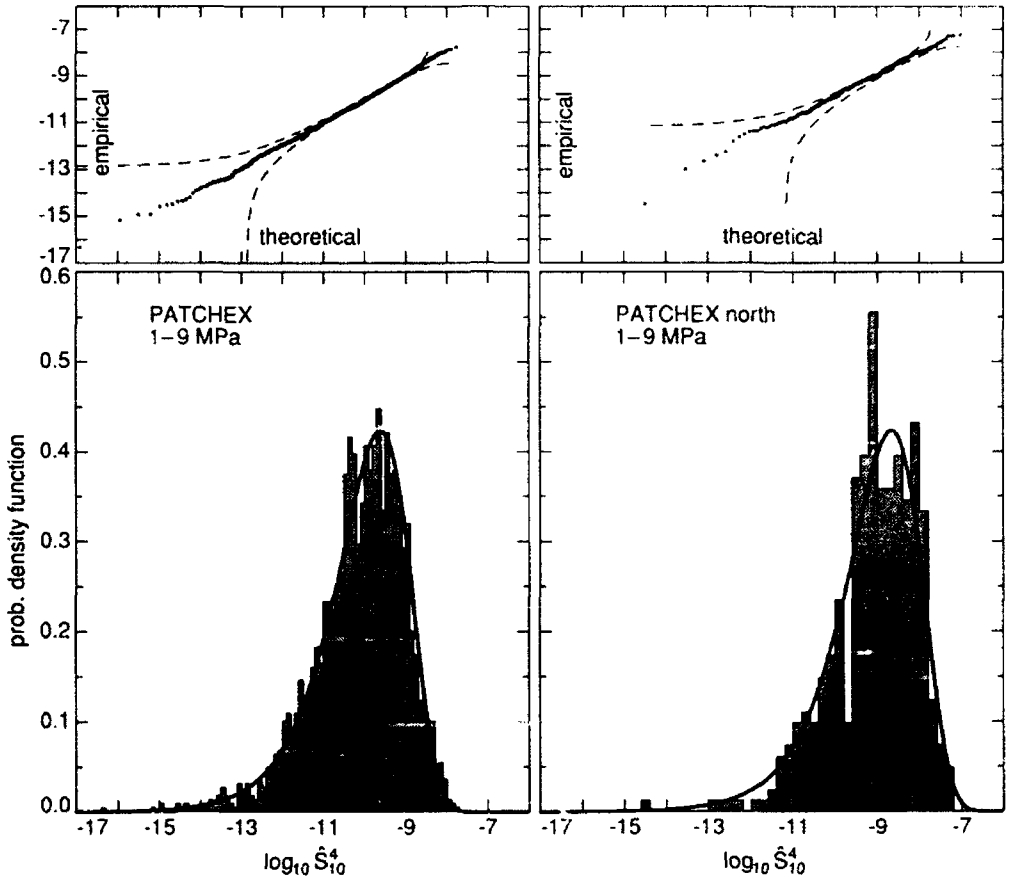

FIG. 5. In the lower panels, the observed distributions of $\log_{10}\hat{S}^4_{10}$ (shaded) agree well with the prediction (B11). In the upper panels, q–q plots based on modified Lilliefors statistics show parts of the PATCHEX distribution slightly exceeding the 95% confidence limits. None of the PATCHEX north distribution falls beyond the bounds.

Distributions that are mostly noise were observed by MSP on the equator during TROPIC HEAT 2 in April 1987. Below the undercurrent, zones several hundred meters thick frequently contain little or no measurable dissipation. In Fig. 6 the distribution of ϵ from 9 to 9.5 MPa during TROPIC HEAT 2 is seen to be similar to the low-magnitude portion of the PATCHEX distribution.

We can estimate the lognormal parameters by fitting the observed histograms to a function that is the sum of the TROPIC HEAT 2 noise distribution and a lognormal distribution. Taking data in increments of 1 MPa, we use a minimum χ^2 procedure to estimate means, $\mu_{\ln\epsilon}$, and standard deviations, $\sigma_{\ln\epsilon}$. These estimates are given as $\tilde{\mu}_{\ln\epsilon}$ and $\tilde{\sigma}_{\ln\epsilon}$. As described in appendix D, the procedure works best for PATCHEX north, which is less affected by noise. For PATCHEX, $\tilde{\mu}_{\ln\epsilon}$ decreases strongly with pressure, and $\tilde{\sigma}_{\ln\epsilon}$ increases gradually from $\tilde{\sigma}_{\ln\epsilon} = 2.9$ at 2–3 MPa to $\tilde{\sigma}_{\ln\epsilon} = 3.2$ at 8–9 MPa (Fig. 7). Its average is 3.01 ± 0.13. For PATCHEX north, $\tilde{\mu}_{\ln\epsilon}$ increases only between 2 and 5 MPa, reflecting the nonuniform vertical distribution of dissipation and shear, and $\tilde{\sigma}_{\ln\epsilon}$ shows no trend and has an average of 2.56 ± 0.17.

b. Averaging 0.5-m ϵ to obtain uncorrelated estimates

Even casual inspection of profiles of 0.5-m ϵ shows vertical trends, with patches of contiguous large values separated by zones at the noise level (Gregg et al. 1986). Consequently, applying the run test to unscaled ϵ between 2.5 and 5.0 MPa, where N is uniform, results in all profiles being rejected (Table 2). Increasing the averaging length, L_z, slowly decreases rejections. For PATCHEX, $L_z = 8$ m yields 3 rejections in 27 profiles, a ratio found previously for random rejections of uncorrelated data (appendix A). Further increasing L_z to 10 m removes all rejections, and we treat 10-m PATCHEX averages as uncorrelated. PATCHEX north requires averaging over 10 to 15 m for no rejections. In both cases, the minimum averaging length required for uncorrelated samples corresponds to the reciprocal of the wavenumber (in cycles per meter) at which the shear spectra roll off (Gregg et al. 1992).

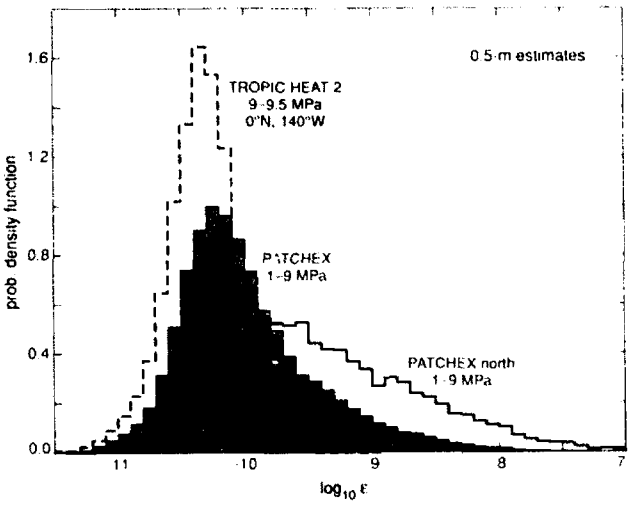

FIG. 6. Probability densities of all 0.5-m $\log_{10}\epsilon$ samples between 1 and 9 MPa for PATCHEX (shaded) and for PATCHEX north (solid line). They are compared with a probability density obtained between 9 and 9.5 MPa on the equator during TROPIC HEAT 2 (dashed line). The latter appears to be nearly all noise.

c. *Noise correction of the 10-m estimates*

To facilitate comparisons of the datasets, we average ϵ over 10 m and scale with $\langle N^2 \rangle$ to form $\hat{\epsilon}$ (3). Testing these profiles for uncorrelatedness over the full range of 1–9 MPa, 11 PATCHEX records fail the run test and 6 fail with the spectral distribution function (Table 3). These failures result from the increasing effect of noise below 5 MPa. To correct for the noise, we set to zero all 0.5-m samples with $\epsilon < 10^{-10}$. Out of 2187 10-m intervals for PATCHEX, 35 have no 0.5-m samples with $\epsilon > 10^{-10}$. Omitting these, only 1 of the PATCHEX profiles fails the run test, but 6 still fail with the spectral distribution function (Table 3). Therefore, a minority of the records have some vertical correlatedness, even after noise correction. Because noise is less important for PATCHEX north, no 10-m intervals had to be dropped, and noise correction does not affect the run test or the spectral distribution function (Table 3). Removing noisy values decreases the magnitudes of the smallest 10-m averages, thereby increasing $\tilde{\sigma}_{\ln\epsilon}$ for both datasets (Table 4).

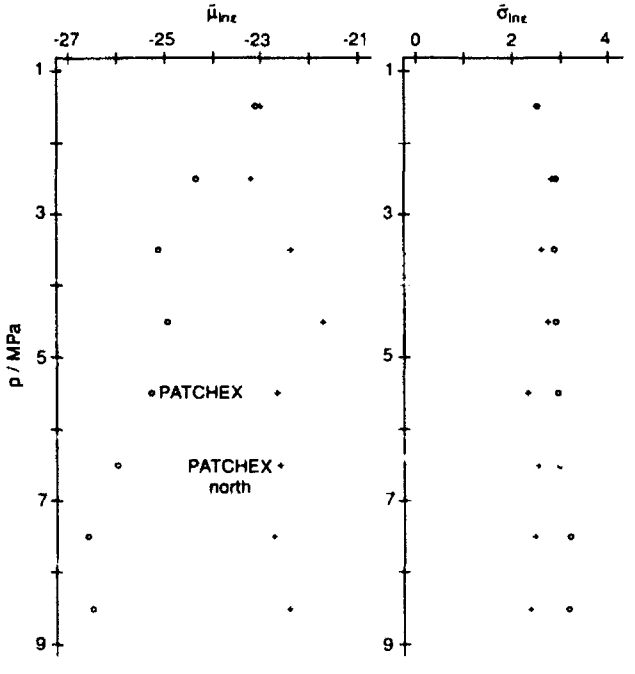

FIG. 7. Parameters for 0.5-m $\ln\epsilon$, obtained by χ^2 fits to data taken in 1 MPa increments. PATCHEX values are shown by open circles and PATCHEX north by crosses. Reflecting different vertical distributions of $\langle\epsilon\rangle$, $\tilde{\mu}_{\ln\epsilon}$ decreases rapidly with pressure for PATCHEX but increases slightly for PATCHEX north. For both datasets, estimates of the standard deviation, $\tilde{\sigma}_{\ln\epsilon}$, are nearly constant below the near-surface high-N duct.

d. *Probability densities of noise-corrected 10-m* $\hat{\epsilon}$

Applying $\langle N^2 \rangle$ scaling to the noise-corrected data affects the standard deviation differently for the two records because they have differing vertical distributions of dissipation (Table 4). Taking the $\langle N^2 \rangle$-scaled and noise-corrected distributions as the most accurate, for PATCHEX the sample mean of $\ln\hat{\epsilon}$, $\tilde{\mu}_{\ln\hat{\epsilon}} = -22.240$ and the sample standard deviation of $\ln\hat{\epsilon}$, $\tilde{\sigma}_{\ln\hat{\epsilon}} = 1.188$; for PATCHEX north $\tilde{\mu}_{\ln\hat{\epsilon}} = -20.270$ and $\tilde{\sigma}_{\ln\hat{\epsilon}} = 1.463$.

After noise correction and $\langle N^2 \rangle$ scaling, both datasets pass q–q tests for lognormality (Fig. 8). With only $\langle N^2 \rangle$ scaling or with only noise correction, neither

TABLE 2. Run tests on averages of 0.5-m ϵ between 2.5 and 5.0 MPa. Because noise contamination is insignificant and the stratification nearly uniform, no corrections are applied to ϵ. The number of rejections is left of the solidus, and the number of samples is right. The number of samples in each profile decreases with increasing averaging length, L_z. All profiles fail for $L_z = 0.5$ m, which represents no averaging; for example, for PATCHEX there are 27 rejections for 27 profiles. Rejections decrease with averaging; there are none for $L_z = 10$ m for PATCHEX and $L_z = 15$ m for PATCHEX north.

L_z/m	n	Rejections
	PATCHEX	
0.5	≤500	27/27
2	125	23/27
4	63	7/27
5	50	6/27
8	32	3/27
10	25	0/27
	PATCHEX north	
5	160	5/5
10	80	2/5
15	80	0/5

TABLE 3. Tests for vertical independence of $\hat{\epsilon}$. Tests on 10-m $\hat{\epsilon}$ between 1 and 9 MPa. SDF refers to the spectral distribution function. The number of rejections is to the left and the number of profiles is to the right.

	Runs rejected	SDF rejected
	PATCHEX	
uncorrected	11/27	6/27
noise corrected	1/27	6/27
	PATCHEX north	
uncorrected	2/5	1/5
noise corrected	2/5	1/5

distribution passes, owing to vertical trends remaining in the profiles. We also scaled with N^1 and $N^{3/2}$, proposed by Gargett (1990) to remove vertical trends. These scalings do not completely remove vertical trends, and owing to the trends the scaled data do not pass for lognormal.

Averaging the 10-m samples over 100 and 800 m reduces $\tilde{\sigma}_{\ln\hat{\epsilon}}$ by factors of 2–3, considerably less than the reduction expected for uncorrelated samples (Table 5). For example, averaging ten of the PATCHEX samples reduces $\tilde{\sigma}_{\ln\hat{\epsilon}}$ from 1.19 to 0.64 instead of to 0.47 as expected. This is similar to the slower-than-expected decrease in $\tilde{\sigma}_{\ln\hat{S}^4_{10}}$.

e. Comparison with probability densities of $\hat{S}^4_{10}$

Scaling the $\hat{S}^4_{10}$ distributions as $\hat{\epsilon}_{1w}$ and overlaying them on the noise-corrected $\hat{\epsilon}$ distributions reveal that both distributions are similar at large magnitudes (Fig. 9). (Appendix E includes a more quantitative comparison using q–q plots.) Agreement at high magnitudes is important because the high-magnitude tails heavily influence the mean values, or first moments. The expected value of $\hat{\epsilon}_{1w}$ is obtained by using (4) and (B3):

$$E[\hat{\epsilon}_{1w}] = 0.959E[\hat{S}^4_{10}] = 0.959 \times 8\sigma^4_\epsilon. \quad (11)$$

It is estimated by $0.959 \times 8\hat{\sigma}^4_\epsilon$. The expected value of $\hat{\epsilon}$ is

$$E[\hat{\epsilon}] \quad \exp(\mu_{\ln\epsilon} + 0.5\sigma^2_{\ln\epsilon}). \quad (12)$$

It is estimated by $\exp(\hat{\mu}_{\ln\epsilon} + 0.5\hat{\sigma}^2_{\ln\epsilon})$. For PATCHEX, the estimate of $E[\hat{\epsilon}_{1w}]$ is 4.65×10^{-10} and the estimate of $E[\hat{\epsilon}]$ is 4.45×10^{-10}. These are within 2% of $\bar{\epsilon}$ $= 4.55 \times 10^{-10}$, the average of the noise-corrected and $\langle N^2 \rangle$-scaled dissipation data. For PATCHEX north, the estimate of $E[\hat{\epsilon}_{1w}]$ is 4.18×10^{-9} and the estimate of $E[\hat{\epsilon}]$ is 4.59×10^{-9}, which are within 20% of $\bar{\epsilon}$ $= 5.13 \times 10^{-9}$.

Because $\hat{\epsilon}$ is much more affected by noise than is $\hat{\epsilon}_{1w}$, their probability densities do not agree at low magnitudes, particularly for PATCHEX (Fig. 9). To demonstrate the effect of noise, we crudely simulated it by adding $5 \times 10^{-11}(N_0/N)^2$ to the 10-m $\hat{S}^4_{10}$ values and then converted them to $\hat{\epsilon}_{1w}$. As seen in the lower panels of Fig. 9, adding the noise greatly improves agreement at low magnitudes.

4. Confidence limits and sampling

a. The second moment of shear, $\hat{S}^2_{10}$

Because $\hat{S}^2_{10}$ is a rescaled χ^2 random variable with two degrees of freedom, confidence limits for $E(\hat{S}^2_{10}) = 2\sigma^2_\epsilon$ can readily be found based on an average of n independent samples, $\langle \hat{S}^2_{10} \rangle \equiv (1/n)\sum_{i=1}^{n} \hat{S}^2_{10,i}$. These limits can be stated as the interval

$$[L_n \times \langle \hat{S}^2_{10} \rangle, \quad U_n \times \langle \hat{S}^2_{10} \rangle]. \quad (13)$$

As shown in appendix E,

$$L_n = \frac{2n}{X^2_{2n,(1+p)/2}} \quad \text{and} \quad U_n = \frac{2n}{X^2_{2n,(1-p)/2}}, \quad (14)$$

where $X^2_{\nu,q}$ is the qth percentage point of the χ^2 distribution with ν degrees of freedom, and p is the confidence level. For $p = 0.95$, averaging 10 samples gives $L_{10} = 0.585$ and $U_{10} = 2.09$ (Fig. 10). As n increases,

TABLE 4. Statistics of 10-m dissipation between 1 and 9 MPa. For both datasets the 10-m estimates are formed in three ways. Arithmetic averages include all 20 of the 0.5-m samples in the 10-m interval. Noise-corrected 10-m values are computed by setting to zero 0.5-m samples less than 10^{-10} W kg^{-3}. For PATCHEX 35 of the 10-m averages contained no values larger than the noise and were dropped from the corrected ensemble. Finally, the noise-corrected estimates are scaled using (3).

Data	n	$\bar{\epsilon}$	$\hat{\mu}_{\ln\epsilon}$	$\hat{\sigma}_{\ln\epsilon}$
		PATCHEX		
arithmetic	2187	4.31×10^{-10}	22.357	1.03
noise corrected	2152	4.02×10^{-10}	22.700	1.373
noise corrected and $\langle N^2 \rangle$ scaled	2152	4.55×10^{-10}	22.240	1.188
		PATCHEX north		
simple average	405	2.12×10^{-9}	20.978	1.303
noise corrected	405	2.10×10^{-9}	21.057	1.408
noise corrected and $\langle N^2 \rangle$ scaled	405	5.13×10^{-9}	20.270	1.463

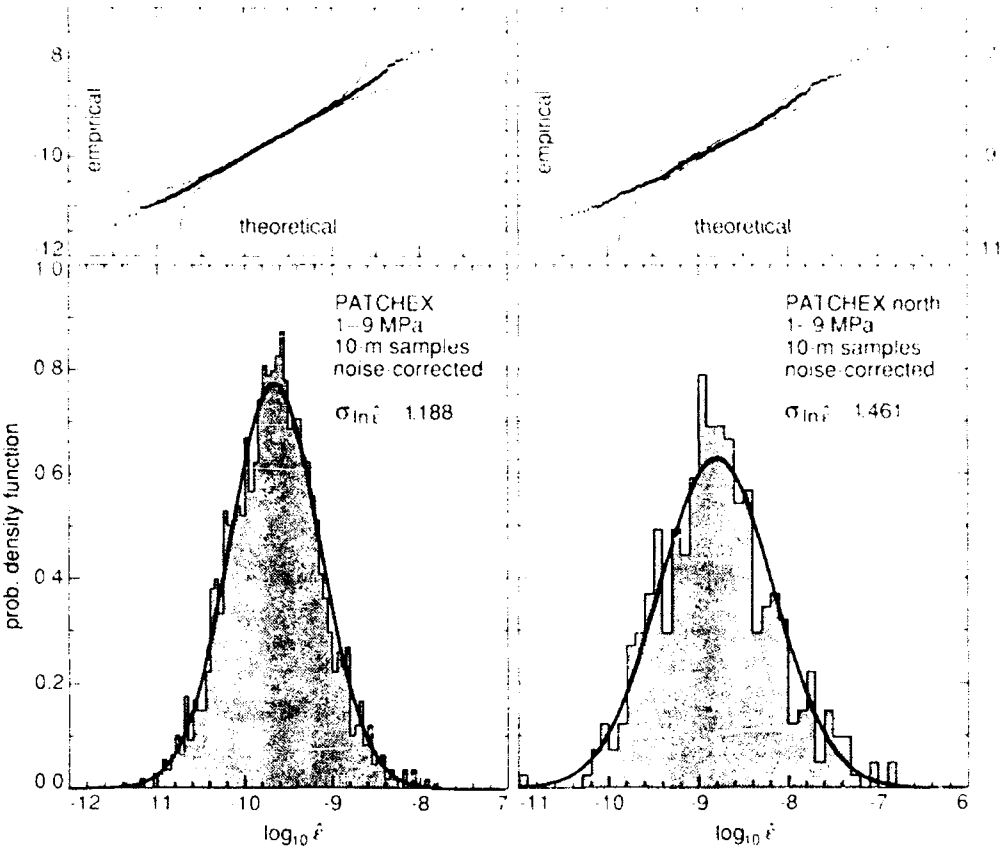

FIG. 8. Probability densities of N^2 -scaled and noise-corrected 10-m dissipation rates. In the lower panels, observed probability densities (shaded) of $\log_{10}\hat{\epsilon}$ are compared with normal distributions having the same means and standard deviations. In the upper panels, q–q plots show that both distributions fall within the 95% confidence limits. To construct the q–q plots, we use the modified Lilliefors test with case 3, estimating means and standard deviations from the distribution.

L_n and U_n slowly converge to 1: averaging the 27 PATCHEX profiles between 500 and 600 m gives $L_{270} = 0.891$ and $U_{270} = 1.13$, and averaging all PATCHEX data having matching noise corrected $\hat{\epsilon}$ yields $L_{2152} = 0.959$ and $U_{2152} = 1.04$.

b. *The fourth moment of shear, $\hat{S}^4_{10}$*

Confidence limits for $E(\hat{S}^4_{10}) = 8\sigma_s^4 = 2[E(\hat{S}^2_{10})]^2$ can also be based on $\langle \hat{S}^2_{10} \rangle$, resulting in

$$[L_n^2 \times 2(\langle \hat{S}^2_{10} \rangle)^2,\ U_n^2 \times 2(\langle \hat{S}^2_{10} \rangle)^2]. \qquad (15)$$

where $2(\langle \hat{S}^2_{10} \rangle)^2$ is an estimate of $\langle \hat{S}^4_{10} \rangle$ for normally distributed shear components. Alternatively, confidence limits can also be based on $\langle \hat{S}^4_{10} \rangle \equiv (1/n) \times \sum_{i=1}^{n} \hat{S}^4_{10,i}$ and take the form

$$[L'_n \times \langle \hat{S}^4_{10} \rangle,\ U'_n \times \langle \hat{S}^4_{10} \rangle]. \qquad (16)$$

As discussed in appendix F, L'_n and U'_n are considerably more difficult to obtain than L_n and U_n. Moreover, for $n > 1$ the expected distance between the upper and lower confidence limits based on $\langle \hat{S}^4_{10} \rangle$ is 3%–12% larger than the expected distance based on $\langle \hat{S}^2_{10} \rangle$. For these reasons, the confidence limits for $E(\hat{S}^4_{10})$ in (15) are preferable.

Because L_n^2 and U_n^2 depend only on n, they are the same for both datasets. Forming the 100-m averages plotted in Fig. 1 requires $n = 10$, resulting in $L^2_{10} = 0.585^2 = 0.342$ and $U^2_{10} = 2.09^2 = 4.36$. Using (4) to convert $\hat{S}^4_{10}$ to $\hat{\epsilon}_m$, we also multiply the multiplicative confidence limits by 0.959. Thus, on the logarithmic axis for $\hat{\epsilon}_m$ in Fig. 1, the 95% confidence limits for the 100-m values correspond to −0.48 and +0.62. For the 800-m averages in Fig. 1, the limits are 0.632 and 1.52, corresponding to −0.20 and +0.18 on the logarithmic axis.

To form confidence limits for the expected value, $E[\hat{\epsilon}_m]$, of all data for each set, for PATCHEX $L^2_{2152} = 0.920$ and $U^2_{2152} = 1.08$. Because the estimate of $E[\hat{\epsilon}_m]$ is 4.65×10^{-10}, the 95% confidence limits are $(4.10 \times 10^{-10}, 4.82 \times 10^{-10})$. Similarly, for PATCHEX north $L^2_{408} = 0.909$ and $U^2_{408} = 1.11$. With an estimate of the expected value equal to 4.18×10^{-9}, 95% confidence limits are $(3.64 \times 10^{-9}, 4.45 \times 10^{-9})$.

TABLE 5. Changes in $\tilde{\mu}_{\ln\hat{\epsilon}}$ and $\tilde{\sigma}_{\ln\hat{\epsilon}}$ with averaging length, L_s. Estimates of sample means and standard deviations of $\ln\hat{\epsilon}$ are given by $\tilde{\mu}_{\ln\hat{\epsilon}}$ and $\tilde{\sigma}_{\ln\hat{\epsilon}}$, respectively. Averaging 10-m noise corrected $\hat{\epsilon}$ over 100 and 800 m increases $\tilde{\mu}_{\ln\hat{\epsilon}}$ and decreases $\tilde{\sigma}_{\ln\hat{\epsilon}}$. For comparison the values in parentheses are the ones expected for averaging fully independent and lognormally distributed 10-m samples. They were calculated by a Taylor series expansion and by Monte Carlo simulation.

	PATCHEX			PATCHEX north		
L_s/m	n	$\tilde{\mu}_{\ln\hat{\epsilon}}$	$\tilde{\sigma}_{\ln\hat{\epsilon}}$	n	$\tilde{\mu}_{\ln\hat{\epsilon}}$	$\tilde{\sigma}_{\ln\hat{\epsilon}}$
10	2152	−22.24	1.19	405	−20.27	1.46
100	216	−21.73 (−21.69)	0.64 (0.47)	40	−19.52 (−19.61)	0.84 (0.60)
800	27	−21.56 (−21.55)	0.23 (0.18)	5	−19.19 (−19.29)	0.36 (0.22)

c. *The dissipation rate, $\hat{\epsilon}$*

For lognormal distributions, $\hat{\epsilon}_{\rm mle}$, the maximum likelihood estimate of $E[\hat{\epsilon}]$ is calculated by evaluating (12) with the sample mean $\tilde{\mu}_{\ln\hat{\epsilon}}$ and sample standard deviation $\tilde{\sigma}_{\ln\hat{\epsilon}}$ of $\ln\hat{\epsilon}$. In appendix G we discuss some difficulties with Baker and Gibson's (1987) use of this estimate.

Land (1975) gives tables for computing exact confidence limits for $E[\hat{\epsilon}]$ based upon $\tilde{\mu}_{\ln\hat{\epsilon}}$ and $\tilde{\sigma}_{\ln\hat{\epsilon}}$. These limits can be written as $[\hat{\epsilon}_{\rm mle}L_n, \hat{\epsilon}_{\rm mle}U_n]$, where L_n and U_n can be obtained from his tables. Land (1972) discusses an approximation to these limits due to D. R. Cox. For 95% confidence limits this approximation takes the simple form

$$[\hat{\epsilon}_{\rm mle}\exp(-1.96\gamma), \hat{\epsilon}_{\rm mle}\exp(1.96\gamma)], \quad (17)$$

where

$$\gamma = [\tilde{\sigma}^2_{\ln\hat{\epsilon}}/n + \tilde{\sigma}^4_{\ln\hat{\epsilon}}/2(n+1)]^{1/2} \quad (18)$$

[Baker and Gibson (1987) obtained a similar result]. While this approximation is useful for large sample

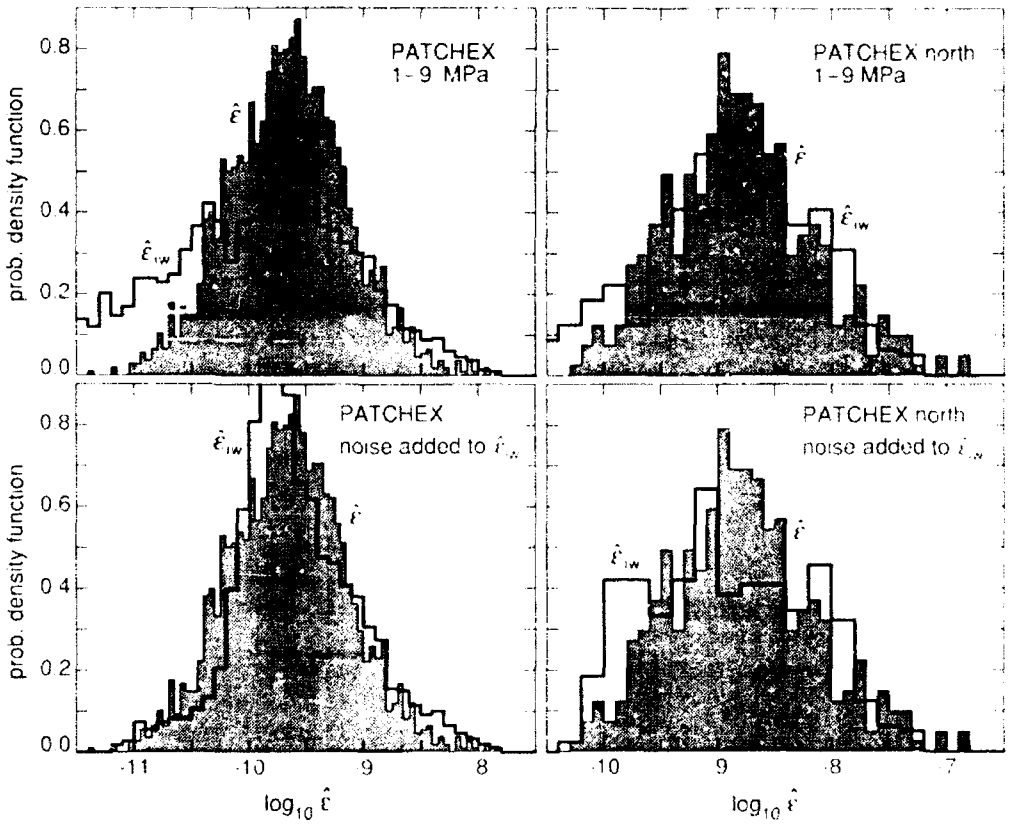

FIG. 9. Comparisons of probability densities of 10-m $\log_{10}\hat{\epsilon}$ (shaded) and $\log_{10}\hat{\epsilon}_{1w}$ (heavy line). The $\hat{\epsilon}$ distributions have been corrected for noise and scaled with $\langle N^2\rangle$. In the upper panels the $\hat{\epsilon}$ and $\hat{\epsilon}_{1w}$ distributions agree much better at high magnitudes than at low magnitudes. The lower panels repeat the comparison after noise similar to that modeled for $\hat{\epsilon}$ has been added to the $\hat{\epsilon}_{1w}$. This greatly improves the overall agreement between the $\hat{\epsilon}$ and $\hat{\epsilon}_{1w}$ probability densities, particularly for PATCHEX.

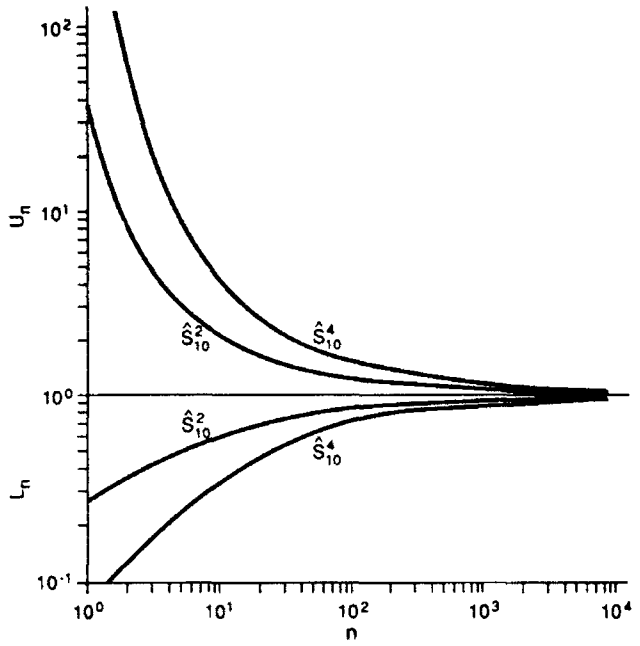

FIG. 10. Multipliers for upper and lower 95% confidence limits of averages of n independent samples of the second and fourth moments of shear. These multipliers are U_n and L_n in (13) for $\hat{S}^2_{10}$ and U^2_n and L^2_n in (15) for $\hat{S}^4_{10}$.

sizes and moderate values of $\tilde{\sigma}_{\ln\hat{\epsilon}}$, it can give large errors for small sample sizes. For example, we take $n = 10$ with $\tilde{\sigma}_{\ln\hat{\epsilon}} = 1.19$ for PATCHEX (Table 5). The approximations give $(0.39\hat{\epsilon}_{\rm mle}, 2.57\hat{\epsilon}_{\rm mle})$ compared to $(0.45\hat{\epsilon}_{\rm mle}, 6.46\hat{\epsilon}_{\rm mle})$ for the exact 95% confidence limits [these limits correspond to $(-0.35 + \log_{10}\hat{\epsilon}_{\rm mle}, +0.81 + \log_{10}\hat{\epsilon}_{\rm mle})$ on logarithmic axes].

The multipliers L_n and U_n are plotted in Fig. 11 for $\sigma_{\ln\hat{\epsilon}} = 0.5$, 1, 1.5, 2, 2.5, and 3, covering the range of $\tilde{\sigma}_{\ln\hat{\epsilon}}$ likely to be obtained from observations. As an example, the values in the first row of Table 5 indicate that $\hat{\epsilon}_{\rm mle} = \exp(-22.24 + 0.5 \times 1.19^2) = 4.45 \times 10^{-10}$ for PATCHEX and $\hat{\epsilon}_{\rm mle} = \exp(-20.27 + 0.5 \times 1.46^2) = 4.57 \times 10^{-9}$ for PATCHEX north. The corresponding 95% confidence limits for $E[\hat{\epsilon}]$ are $(4.17 \times 10^{-10}, 4.76 \times 10^{-10})$ for PATCHEX (based upon $n = 2152$ samples) and $(3.76 \times 10^{-9}, 5.69 \times 10^{-9})$ for PATCHEX north ($n = 405$ samples). The corresponding multipliers are $L_{2152} = 0.937$ and $U_{2152} = 1.07$ for PATCHEX and $L_{405} = 0.823$ and $U_{405} = 1.25$ for PATCHEX north. For both datasets the confidence limits include the estimates obtained using $\tilde{\sigma}^4_\epsilon$ in (11) and the computed sample averages of $\hat{\epsilon}$.

5. Summary and discussion

a. Summary

Statistics of shear and dissipation are compared for two sets of profiles taken when the internal wave field appeared statistically homogeneous over distances of kilometers and steady over intervals of days. For one set, PATCHEX, the internal waves are close to GM76; for the other set, PATCHEX north, the root-mean-square 10-m shear is three times GM76. Our findings are as follows.

1) After scaling the shear components, S_x and S_y, with $\langle N^2 \rangle$, the scaled components, $\hat{S}_x$ and $\hat{S}_y$, are normally distributed with zero means and are uncorrelated with each other. This readily leads to analytic forms for the probability density functions of $\hat{S}^2_{10}$ and $\hat{S}^4_{10}$. The latter is highly skewed, and the standard deviation of $\ln\hat{S}^4_{10}$ is a constant, $\sigma_{\ln\hat{S}^4_{10}} = 2.57$. For PATCHEX north the measured distributions of $\hat{S}^2_{10}$ and $\hat{S}^4_{10}$ are within the 95% confidence limits of the analytic forms. For PATCHEX the measured distributions are similar to the analytical forms, but they slightly exceed the 95% limits.

2) For both datasets the probability densities of the inverse Richardson number, $\mathrm{Ri}^{-1}_{10} \equiv S^2_{10}/\langle N^2 \rangle$, are close to those predicted. Consistent with Eriksen (1978), the PATCHEX distribution cuts off near 4, but 9% of the PATCHEX north distribution has $\mathrm{Ri}^{-1}_{10} > 4$. Therefore, the cutoff at $\mathrm{Ri}^{-1}_{10} = 4$ is not a universal constraint.

3) For bulk ensembles of 0.5-m ϵ collected where $\langle N^2 \rangle$ is nearly constant, the lognormal parameters, $\mu_{\ln\epsilon}$ and $\sigma_{\ln\epsilon}$, can be estimated objectively by minimiz-

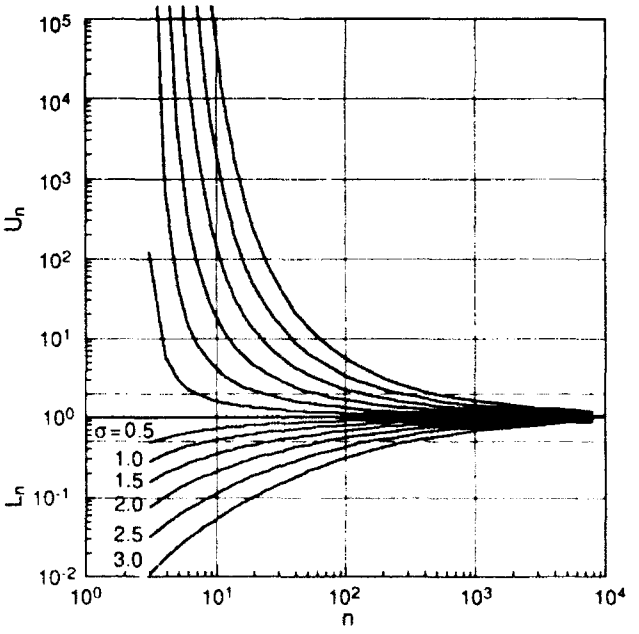

FIG. 11. Multipliers for upper (U_n) and lower (L_n) 95% confidence limits of averages of lognormal distributions, as functions of the number of samples, n, and of the standard deviation of the natural logarithm of the variable. The multipliers are obtained by interpolating the exact confidence limits given by Land (1975) and are given for $\sigma_{\ln\epsilon}$ spanning the range expected in the ocean.

ing χ^2 fits to the sum of a lognormal distribution and an empirically determined noise distribution. In our cases, the noise distribution was observed in an unusually quiet section below the equatorial undercurrent. Fits to 0.5-m ϵ taken in bins of 1 MPa vary in quality and have averages of $\tilde{\sigma}_{\ln\epsilon}$ equaling 3.01 ± 0.13 for PATCHEX and 2.56 ± 0.17 for PATCHEX north.

4) Half-meter ϵ are not uncorrelated but must be averaged vertically to form uncorrelated samples. The minimum averaging length is 10 m for PATCHEX and about 15 m for PATCHEX north. Both averaging lengths correspond approximately to the reciprocal of the wavenumber at which their respective shear spectra roll off (Gregg et al. 1992).

5) After correcting for noise and scaling ϵ with $\langle N^2 \rangle$, probability densities of 10-m N-scaled dissipation rates, $\hat{\epsilon}$, are lognormal. [Scaling with $\langle N^1 \rangle$ and $\langle N^{3/2} \rangle$ does not yield lognormality.] Thus, the logarithms of 10-m scaled dissipation are normal. As they are also uncorrelated, they can be assumed to be independent. These distributions have $\tilde{\sigma}_{\ln\hat{\epsilon}} = 1.19$ for PATCHEX and 1.46 for PATCHEX north. The 10-m samples, however, are not fully independent; namely, further averaging does not reduce $\tilde{\sigma}_{\ln\hat{\epsilon}}$ as rapidly as expected for independent samples. This appears to be the result of weak vertical correlation within profiles and temporal correlation between profiles.

6) For 10-m samples, the probability densities of 10-m $\log\hat{\epsilon}$ and $\log\hat{S}^4_{10}$ (represented as $\log\hat{\epsilon}_{10}$) are similar at high magnitudes, and mean values of $\hat{\epsilon}$ and $\hat{\epsilon}_{10}$ differ by only 2%–20%. As a consequence of the frequent lack of turbulence at low shear magnitudes, noise affects much of the low-magnitude probability density of $\hat{\epsilon}$, causing it to differ from the $\hat{\epsilon}$ distribution.

7) Our assumption that the data result from random processes appears valid since the confidence limits capture the collapse with averaging (Fig. 1). This also lends credence to our approach in testing for independence.

8) Ten independent measurements are needed to obtain 95% confidence limits of a factor of 2 for $E(\hat{S}^2_{10}) = 2\sigma^2_{\hat{S}^2}$. Owing to the higher skewness of its distribution, similar confidence limits for $\hat{S}^4_{10}$ require as few as 40 independent samples. Sixty independent dissipation samples are also needed for the same degree of confidence in 10-m dissipation rates (these are computed using $\tilde{\sigma}_{\ln\hat{\epsilon}} \leq 1.5$ in maximum likelihood estimates for $E[\hat{\epsilon}]$). Tightening the confidence limits rapidly increases the number of samples required.

b. Discussion

We average and then decimate to obtain independent samples. As a reviewer correctly notes, independent samples can also be obtained by decimation without averaging. Although decimation-only is suitable for some studies, we need to average and decimate to retain the average dissipation accompanying the internal wave shear over the same vertical interval. Also, 10-m averaged $\hat{\epsilon}$ data approximately follow a lognormal distribution, whereas the unaveraged 0.5-m data follow at best a complicated lognormal plus noise model. Since decimation leaves the underlying distribution of the data unchanged, it is easier to provide a tractible statistical model for averaged data than for decimated data.

Why are the high-magnitude portions of ϵ probability densities lognormal or nearly so? Dissipation is lognormal or approximately so in homogeneous turbulence; in the thermocline, ϵ can be lognormal within individual turbulent patches if the sample length is at least three times the Kolmogoroff length but much smaller than the height of the patch (Yamazaki and Lueck 1990). Most ensembles of thermocline data, however, consist of records taken minutes to days apart over distances of tens to hundreds of meters in the vertical and hundreds of meters to tens of kilometers in the horizontal. Consequently, the samples come from places with no turbulence as well as from many different turbulent patches. Furthermore, the patches are probably produced by a variety of mechanisms and are observed at varying stages in their life cycles. As a result, these bulk ensembles do not satisfy the assumptions made in deriving lognormal distributions for homogeneous turbulence (Gurvich and Yaglom 1967) or within individual patches in the thermocline (Yamazaki and Lueck 1990). As also noted for χ (Gregg 1980) as well as for ϵ (Gibson 1981), the bulk statistics of χ and ϵ are likely to be approximately lognormal simply because they have multiplicative rather than additive probabilities. Based on the similarity of the high-magnitude portions of probability densities of $\hat{\epsilon}$ and $\hat{S}^4_{10}$, we suggest that lognormality of $\hat{\epsilon}$ may be an approximate condition resulting from the production of turbulence in proportion to skewed higher moments of internal wave shear. A rigorous lognormal model may be possible, but we do not know enough to construct one.

Because most turbulence in the thermocline is produced by breaking internal waves, the statistics of bulk ensembles of ϵ must reflect the character of internal waves as well as the inherent intermittence of turbulence. Whether or not the fourth shear moment is the best model, $\hat{\epsilon}$ depends on a skewed shear moment that resembles some characteristics of the lognormal distribution. With only two datasets, we obviously have not proven this relationship, but consider it a hypothesis to be tested.

If these results are substantiated by further observations, they have several consequences. First, the spread of the distribution of $\hat{S}^4_{10}$ (or some other higher moment) should be an approximate upper bound for the spread of the $\hat{\epsilon}$ distribution. It is an upper bound because the low-magnitude portion of the shear distribution on average does not produce turbulence or

it generates only low ϵ's. Consistent with this, for the independent 10-m samples we observe $\hat{\sigma}_{\ln\hat{S}} = 1.19$ for PATCHEX and 1.49 for PATCHEX north, significantly less than $\sigma_{\ln S^4_{10}} = 2.57$. The spread for PATCHEX north is the larger because the dissipations are larger and less affected by noise. Comparing shear measurements at 12 sites in the Atlantic and Pacific, Smart (1988) reports $E = 1$–10 times GM76. As $\hat{S}^2_{10} \propto E$, the more energetic of these sites should test our hypothesis that 2.57 is an upper bound for $\sigma_{\ln\hat{S}}$ produced by internal wave shear. Second, if lognormality is only an approximate condition, lognormal statistics should not be relied on a priori, as datasets may approach lognormality to varying degrees. Third, the statistics of dissipation are likely to differ considerably when turbulent production results from processes other than random internal wave fields. For example, our development does not apply to turbulence produced by hydraulic jumps or solitary waves, such as those in the Strait of Gibraltar.

As a consequence of the dependence of microstructure statistics on the internal wave field, microstructure measurements from different times and places cannot be combined into a single ensemble for statistical analysis. For example, Gregg (1977) compares three sets of Cox numbers obtained during different seasons at 28°N, 155°W and notes that their variability suggests modulation of microstructure intensity by mesoscale eddies or seasonal effects. Subsequently, Briscoe and Weller (1984) reported an apparent yearly cycle in the energy of high-frequency internal waves in which E varies by factors of 2–3 about the long-term mean. Nevertheless, Baker and Gibson (1987) combined the three sets of Cox numbers into a single ensemble without considering whether the three sets were independent. Proper treatment would consider each cruise as an ensemble with its own statistics and then examine the statistics of the grand average.

How much sampling is optimum for $\hat{\epsilon}$? The 27 PATCHEX profiles give $L_{2152} = 0.937$ and $U_{2152} = 1.07$ compared with $L_{405} = 0.823$ and $U_{405} = 1.25$ for the 5 PATCHEX north profiles. Because we do not believe our calibrations are better than the PATCHEX north confidence limits, the additional sampling during PATCHEX did not improve our overall confidence in the averages. If our objective had been to estimate whether a large area had a vertical eddy diffusivity of 10^{-4} or 10^{-5} m^2 s^{-1}, a more accurate result would have been obtained by sampling to obtain ±100% accuracy at each of many sites. The sites should be separated by about 20 km, the approximate correlation distance for internal wave statistics (D'Asaro and Perkins 1984). Assuming $\sigma_{\ln\hat{S}} = 1.2$–2.57 requires $n = 33$–282, equivalent to 1–4 MSP profiles per site for ±100% accuracy. If $\sigma_{\ln\hat{S}} = 1.5$, specifying ±10% accuracy for 95% confidence limits, as in the abstract of Baker and Gibson (1987), increases sampling requirements from $n = 60$ to $n = 2000$, or 25 MSP profiles per site instead of only one.

Acknowledgments. The Office of Naval Research funded collection of these data under Contract N00014-84-C-0111 and analysis under Contract N00014-86-K-0690, which supported the Mixing to Mesoscale University Research Initiative. H. Yamazaki and D. Winkel gave valuable comments, and we are indebted to the reviewer of an earlier version of the paper whose comment "Statistical bafflegab is no substitute for physics . . . garbage in, garbage out as they say" strengthened our resolve to improve the statistical training of oceanographers.

APPENDIX A

Details on Statistical Tests

a. Vertical uncorrelatedness of shear components

To examine the vertical correlation structure of $\hat{S}_z$ or $\hat{S}_x$, we apply the run test and the spectral distribution function separately. The run test is a simple nonparametric test of uncorrelatedness (Bendat and Piersol 1971). A run is a sequence of consecutive values lying on one side of the median. If the n values in the series are random and independent, the number of runs, R, is a random variable with an expected value

$$E(R) = (2n_+n_-/n) + 1 \qquad \text{(A1)}$$

and a variance

$$\sigma^2_R = [2n_+n_-(2n_+n_- - n)]/[n^2(n-1)], \qquad \text{(A2)}$$

where n_+ and n_- are the number of values greater and less than the median, and $n = n_+ + n_-$. For large n, $E(R) \approx n/2$ and $\sigma_R \approx \sqrt{n}/4$. The hypothesis of uncorrelatedness can be rejected at the 5% level of significance if R is outside the interval

$$(E(R) - 1.96\sigma_R, E(R) + 1.96\sigma_R). \qquad \text{(A3)}$$

For instance, each profile contains 81 $\hat{S}_z$ samples between 1 and 9 MPa, leading us to expect 40.5 runs in each record with 95% confidence limits of (32.2, 49.8).

We applied the run test to all $\hat{S}_z$ profiles and to all $\hat{S}_x$ profiles. For PATCHEX, R lies outside the 95% confidence limits in three $\hat{S}_z$ and four $\hat{S}_x$ profiles (Table A1). For PATCHEX north, on the other hand, one $\hat{S}_z$ and three $\hat{S}_x$ profiles are out of bounds. For comparison, with a level of significance of 5% and with truly uncorrelated data, we expect incorrect rejections in approximately $0.05 \times 27 = 1.35$ profiles out of 27. The number of incorrect rejections itself varies about its expected value. To assess the magnitude of this variation, we simulated normally distributed white noise with zero mean and the same standard deviation as

TABLE A1. Tests for independence. The run test (RT) for a profile is rejected as containing independent samples when R, the number of runs, exceeds the 95% confidence limits (A3). The spectral distribution function (SDF) of a profile is rejected when any point exceeds the 95% confidence limits for the Kolmogoroff-Smirnoff test. The number of rejections is left of the solidus, and the number of runs is right. Only for $\hat{S}_x$ and $\hat{S}_y$ for PATCHEX north is the same profile (MSP 120) rejected by both tests. Each profile contains 81 samples of 10-m shear.

	Rejected by RT	Rejected by SDF	Rejected by both
	PATCHEX		
$\hat{S}_x$	3/27	0/27	0/27
$\hat{S}_y$	4/27	2/27	0/27
$\hat{S}^2_{10}$	2/27	2/27	0/27
$\hat{S}^4_{10}$	2/27	1/27	0/27
	PATCHEX north		
$\hat{S}_x$	1/5	2/5	1/5
$\hat{S}_y$	3/5	2/5	1/5
$\hat{S}^2_{10}$	0/5	0/5	0/5
$\hat{S}^4_{10}$	0/5	0/5	0/5

the shear components. We grouped the simulated data into 27 profiles of 81 samples each and applied the run test in the same fashion as we did with the real PATCHEX data. By repeating this procedure 1467 times, we observed 2 or more rejections out of 27 profiles in 34% of the repetitions; 3 or more in 12% of the repetitions; and 4 or more in 3% of the repetitions (the maximum number of rejections we observed was 6). Therefore, the number of rejections for PATCHEX does not suggest gross departures from uncorrelatedness for $\hat{S}_x$ or for $\hat{S}_y$. This is not true, however, for PATCHEX north; rejections exceed the number expected by chance, indicating vertical correlatedness in both $\hat{S}_x$ and $\hat{S}_y$.

The second test uses the spectral distribution function, which is the cumulative integral of the spectral density function. (The empirical version of this function is known as the cumulative periodogram.) Uncorrelated samples have a white (flat) spectral density function and, equivalently, a linear spectral distribution function. Consequently, an empirical spectral distribution function of uncorrelated data should fluctuate about a straight line, and this is used to test for uncorrelatedness (Jenkins and Watts 1969). A profile is rejected as being white if any point of its spectral distribution function departs from the expected straight line by more than the 95% confidence limits using the Kolmogoroff-Smirnoff test (Fig. A1). As is evident in Table A1, the number of rejections is similar to that for the run test, but the pattern of rejections is random. Only one $\hat{S}_x$ and one $\hat{S}_y$ profile are rejected by both tests, which we take as further evidence for no gross departures from uncorrelatedness.

b. *Uncorrelatedness between simultaneous shear components*

Taking all pairs of $\hat{S}_x$ and $\hat{S}_y$ for each cruise, we compute Spearman's rank-order correlation coefficient and Kendall's τ. Both coefficients are well-accepted nonparametric tests whose validity does not depend on the assumption of normality (Conover 1980). We compute the coefficients using numerical routines of Press et al. (1988). In all cases we cannot reject (at the 0.05 level of significance) the null hypothesis that $\hat{S}_x$ and $\hat{S}_y$ are uncorrelated. Neither test comes close to rejecting the null hypothesis; the closest is Kendall's $\tau = 0.0133$ for PATCHEX, which can be rejected only at the 35% level of significance. For comparison, $\tau = -0.0067$ for PATCHEX north can be rejected only with an 84% level of significance. Therefore, we can treat $\hat{S}_x$ and $\hat{S}_y$ as uncorrelated with each other.

c. *Lilliefors statistics for 95% confidence limits on q–q plots*

The 95% confidence limits are derived from Lilliefors statistics for normal or exponential distributions (Mason and Bell 1986). The Lilliefors statistic is a modification of the Kolmogoroff–Smirnoff statistic to compensate for using estimated parameters. Computed by Monte Carlo simulations, the modification generally gives a smaller acceptance region when parameters must be estimated than when they are assumed to be known. Mason and Bell extend previous calculations by Stephens (1974) for estimated parameters and revise Stephens' critical values using improved Monte Carlo techniques. For $\hat{S}_x$ and $\hat{S}_y$ in Fig. 2, we assume a known mean of zero, corresponding to normal case 2 of Mason and Bell. For q–q plots of $\hat{S}^2_{10}$ and $\hat{S}^4_{10}$, we use the ex-

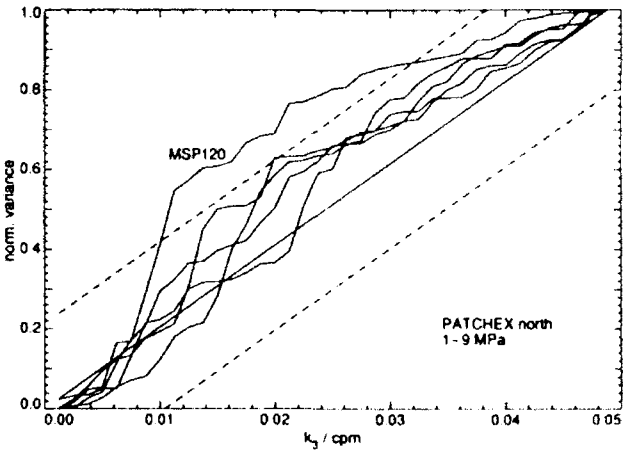

FIG. A1. Spectral distribution functions (aka cumulative periodograms) for PATCHEX north $\hat{S}_x$ profiles. Cumulative variances, normalized to maxima of one, are plotted on the y axis versus vertical wavenumber on the x axis. Spectral distribution functions of white noise would plot along the diagonal. The dashed lines are 95% confidence limits of the modified Kolmogoroff–Smirnoff test.

ponential case. For $\hat{\epsilon}$, we must estimate both the mean and standard deviation from the observed distribution and use case 3 of Mason and Bell.

APPENDIX B

Derivation of Probability Densities

a. Probability density of $\hat{S}^2_{10}$

Rather than comparing the probability density of $\hat{S}^2_{10}$ with observations, it is more convenient to use $z \equiv \log_{10}\hat{S}^2_{10} = \ln\hat{S}^2_{10}/\ln 10$. Following standard procedures (Papoulis 1984), we take $y \equiv \hat{S}^2_{10}$ and

$$G(y) = z = \log_{10} y = \log_{10}\hat{S}^2_{10} = \ln\hat{S}^2_{10}/\ln 10.$$

It has one root, $y_1 = e^{z \ln 10}$, and the derivative of the function is $G'(y) = 1/(y \ln 10)$. Consequently,

$$P_z = \frac{P_y(y_1)}{|G'(y_1)|} = \frac{\ln 10\, e^{z \ln 10} e^{-e^{z \ln 10}/2\sigma_s^2}}{2\sigma_s^2}. \quad \text{(B1)}$$

b. Probability density of $\hat{S}^4_{10}$

Following the same procedures, we return to (8) to obtain the probability density of $\hat{S}^4_{10}$. Defining $w \equiv g(y) = y^2$, y has only one positive root, $y_1 = \sqrt{w}$. Therefore,

$$P_w = \frac{P_y(y_1)}{|g'(y_1)|} = \frac{\exp(-y/2\sigma_s^2)}{4y\sigma_s^2} \quad \text{for } y \geq 0,$$

$$w \equiv y^2 = \hat{S}^4_{10}. \quad \text{(B2)}$$

The first and second moments are

$$E[w] = \int_{-\infty}^{\infty} wP_w dw = 8\sigma_s^4 \quad \text{(B3)}$$

and

$$E[w^2] = \int_{-\infty}^{\infty} w^2 P_w dw = 384\sigma_s^8. \quad \text{(B4)}$$

Therefore, the variance of $\hat{S}^4_{10}$ is also a simple function of σ_s,

$$\sigma_w^2 = E[w^2] - (E[w])^2 = 320\sigma_s^8, \quad \text{(B5)}$$

and the standard deviation is always 2.2 times the mean, $\sigma_w = 17.9\sigma_s^4 = 2.2E[w]$.

For later use with lognormal statistics, we define $z \equiv h(w) = \ln w$, which has one root, $w_1 = e^z$. Then

$$P_z = \frac{P_w(w_1)}{|h'(w_1)|} = \frac{\sqrt{e^z}e^{-\sqrt{e^z}/2\sigma_s^2}}{4\sigma_s^2}, \quad z \equiv \ln w = \ln\hat{S}^4_{10}, \quad \text{(B6)}$$

and the first moment is

$$E[z] = \ln(4\sigma_s^4) - 2\gamma, \quad \text{(B7)}$$

where $\gamma = 0.57721\cdots$ is the Euler constant. The second moment is

$$E[z^2] = \ln^2(4\sigma_s^4) - 4\gamma \ln(4\sigma_s^4) + 4\left(\frac{\pi^2}{6} + \gamma^2\right) \quad \text{(B8)}$$

yielding

$$\sigma_z^2 = (2/3)\pi^2, \quad \text{(B9)}$$

or

$$\sigma_z = \sigma_{\ln\hat{S}^4_{10}} = 2.57. \quad \text{(B10)}$$

Therefore, $\sigma_{\ln\hat{S}^4_{10}}$ is constant, independent of variations in σ_s.

To compare this with observed distributions, we plot

$$P_{zz} = \frac{\ln 10\sqrt{e^{zz - \log_{10} e}}\, e^{-\sqrt{e^{zz - \log_{10} e}}/2\tilde{\sigma}_s^2}}{4\tilde{\sigma}_s^2},$$

$$zz \equiv \log_{10} w = \log_{10}\hat{S}^4_{10}. \quad \text{(B11)}$$

Using (4) to scale $\hat{S}^4_{10}$ as $\hat{\epsilon}_{iw}$, the logarithmic form is

$$P_t = \frac{\ln 10\sqrt{e^{t \ln 10}}\, e^{-\sqrt{e^{t \ln 10}}/2\tilde{\sigma}_s^2}}{4c\tilde{\sigma}_s^2}, \quad t \equiv \log_{10}\hat{\epsilon}_{iw}. \quad \text{(B12)}$$

APPENDIX C

Statistics of $\hat{S}^2_{10}$ and $\hat{S}^4_{10}$

a. Vertical uncorrelatedness of $\hat{S}^2_{10}$ and $\hat{S}^4_{10}$

No PATCHEX north profiles are rejected by the run test or by the spectral distribution function (Table A1), and only 2 of the 27 PATCHEX profiles are rejected, none by both tests. Consequently, these tests give no indication of significant correlatedness in $\hat{S}^2_{10}$ and $\hat{S}^4_{10}$. Presumably, the moments have fewer rejections than the shear components because they depend on both $\hat{S}_x$ and $\hat{S}_y$, which are uncorrelated with each other.

b. Temporal correlatedness

To examine temporal correlation for PATCHEX, we average $\hat{S}_x$, $\hat{S}_y$, $\hat{S}^2_{10}$, and $\hat{S}^4_{10}$ over 100-m segments chosen to minimize decorrelation due to vertical displacements by internal waves and the internal tide. This results in eight time series for each parameter, with each set containing 27 values, one for each profile. None of the run tests for $\hat{S}_x$ or $\hat{S}_y$ must be rejected, but two of the eight series for $\hat{S}^2_{10}$ and $\hat{S}^4_{10}$ must be rejected.

c. Decrease in variances with averaging

The probability densities of $\hat{S}^2_{10}$ and $\hat{S}^4_{10}$ allow us to predict how arithmetic averaging reduces the variances

TABLE C1. Decrease in $\tilde{\alpha}$ with averaging length, L_z. In each column the observed values of $\tilde{\alpha}_{\ln S^2_{10}}$ or $\tilde{\alpha}_{\ln S^4_{10}}$ are given first and followed in parentheses by the analytic values determined from (C2), (C3), and (C4). Also within the parentheses are standard deviations of the estimates as determined from Monte Carlo simulations.

	PATCHEX		PATCHEX north	
L_z (m)	$\tilde{\alpha}_{\ln S^2_{10}}$	$\tilde{\alpha}_{\ln S^4_{10}}$	$\tilde{\alpha}_{\ln S^2_{10}}$	$\tilde{\alpha}_{\ln S^4_{10}}$
10	1.27 (1.28 ± 0.03)	2.55 (2.56 ± 0.05)	1.18 (1.28 ± 0.07)	2.36 (2.56 ± 0.13)
100	0.42 (0.32 ± 0.02)	0.85 (0.68 ± 0.03)	0.32 (0.32 ± 0.04)	0.62 (0.67 ± 0.08)
800	0.19 (0.11 ± 0.02)	0.33 (0.24 ± 0.03)	0.17 (0.11 ± 0.03)	0.33 (0.21 ± 0.08)

of these moments. Owing to the large skewness of the probability densities, we describe the variances with $\sigma^2_{\ln S^2_{10}}$ and $\sigma^2_{\ln S^4_{10}}$, which also facilitates comparing shear variances with variances of $\hat{\epsilon}$.

If the shear components are independent, $\hat{S}^2_{10}$ is distributed as an χ^2 random variable with two degrees of freedom; that is,

$$\hat{S}^2_{10,i} \overset{d}{=} c\chi^2_2, \tag{C1}$$

where $\hat{S}^2_{10,i}$ represents the 10-m shear variances for $i = 1$–2187, and $\hat{S}^2_{10,i}$ and $\hat{S}^2_{10,j}$ are independent for $i \neq j$. Then

$$\sigma^2_{\ln S^2_{10}} = \mathrm{var}(\ln \hat{S}^2_{10,i}) = \mathrm{var}(\ln(c\chi^2_2)) = \mathrm{var}(\ln \chi^2_2). \tag{C2}$$

That is, the proportionality factor, c, does not affect the variance.

These variances are given analytically (Bartlett and Kendall 1946) as

$$\mathrm{var}(\ln \chi^2_{2K}) = \psi'(K), \tag{C3}$$

where $\psi'(K)$ is the derivative of the digamma function (sometimes called the trigamma function). For $K = 1$ we have $\psi'(1) = \pi^2/6$, yielding $\sigma_{\ln S^2_{10}} = \pi/\sqrt{6} = 1.28$. This is in good agreement with the observed PATCHEX data and within 10% of the observed PATCHEX north data (Table C1). We use Monte Carlo methods to assess the expected variability in estimates of $\mathrm{var}\{\ln \chi^2_{2K}\}$.

When averaging $\hat{S}^2_{10,i}$ over 100 and 800 m, we are adding independent scaled χ^2 random variables with two degrees of freedom, yielding scaled χ^2 random variables with more degrees of freedom. Therefore, we have

$$\mathrm{var}\left(\ln\left[\frac{1}{10}\sum_{i=1}^{i=10}\hat{S}^2_{10,i}\right]\right) = \mathrm{var}(\ln \chi^2_{20})$$

$$\mathrm{var}\left(\ln\left[\frac{1}{80}\sum_{i=1}^{i=80}\hat{S}^2_{10,i}\right]\right) = \mathrm{var}(\ln \chi^2_{160}). \tag{C4}$$

For the 100-m PATCHEX averages and for all of the 800-m averages, the observed variances exceed the predictions (Table C1)—in some cases as much as 50%. The discrepancies are largest for the 800-m averages, suggesting that a weak temporal coherence may be partly responsible. In view of the discrepancies, the increase in degrees of freedom with averaging is not as large as expected.

APPENDIX D

Assessing the Lognormal Plus Noise Model

We investigate the hypothesis that the 0.5-m uncorrected ϵ data in a particular depth range can be regarded as the summation of (1) a lognormally distributed random variable with parameters $\mu_{\ln\Lambda}$ and $\sigma_{\ln\Lambda}$ and (2) random noise. Specifically, we assume that $\epsilon = \Lambda + N$, where Λ is a lognormal random variable with

$$E\{\Lambda\} = e^{\mu_{\ln\Lambda} + \sigma^2_{\ln\Lambda}/2} \quad \text{and} \quad \mathrm{var}\{\Lambda\} = E\{\Lambda^2\} - (E\{\Lambda\})^2 = e^{2\mu_{\ln\Lambda} + \sigma^2_{\ln\Lambda}}(e^{\sigma^2_{\ln\Lambda}} - 1). \tag{D1}$$

That is, $\ln(\Lambda)$ is Gaussian distributed with mean $\mu_{\ln\Lambda}$ and variance $\sigma^2_{\ln\Lambda}$. The noise variate N is assumed to be independent of Λ and to follow the observed distribution from TROPIC HEAT 2 between 9 and 9.5 MPa. By ordering $M = 1480$ noise values as $n_1 < n_2 < \cdots < n_M$ and assuming each equally likely, the probability of a value less than n_i is

$$\mathrm{P}[N \leq n_i] = \frac{i}{M}. \tag{D2}$$

We next determine the cumulative distribution function for observations of dissipation plus noise,

$$\begin{aligned} F_\epsilon(x) &= \mathrm{P}[\epsilon \leq x] = \mathrm{P}[\Lambda + N \leq x] \\ &= \sum_{i=1}^{M} \mathrm{P}[\Lambda + N \leq x \text{ and } N = n_i] \\ &= \sum_{i=1}^{M} \mathrm{P}[\Lambda + N \leq x | N = n_i]\,\mathrm{P}[N = n_i] \\ &= \frac{1}{M}\sum_{i=1}^{M} \mathrm{P}[\Lambda \leq x - n_i] \\ &= \frac{1}{M}\sum_{i=1}^{M} F_\Lambda(x - n_i). \end{aligned} \tag{D3}$$

where $F_\Lambda(\cdot)$ is the cumulative distribution function of the lognormally distributed variate Λ; that is,

$$F_\Lambda(x - n_j) = \begin{cases} \Phi\left(\dfrac{\ln(x - n_j) - \mu_\Lambda}{\sigma_\Lambda}\right), & \text{if } x > n_j \\ 0, & \text{otherwise,} \end{cases} \quad \text{(D4)}$$

and $\Phi(\cdot)$ is the cumulative distribution function for a Gaussian random variable with zero mean and unit variance.

Given a sample $\epsilon_1, \epsilon_2, \ldots, \epsilon_L$ of ϵ measurements in a particular depth range, we fit our model using a minimum chi-square procedure (Conover 1980, pp. 195–197). We use K bins bounded by x_{i-1} and x_i such that

$$0 \equiv x_0 < x_1 < x_2 < \cdots < x_{K-1} < x_K \equiv \infty. \quad \text{(D5)}$$

The kth class of observations for $k = 1$ up to K is defined to be the set of all ϵ measurements satisfying $x_{k-1} \leq \epsilon_l < x_k$. Let O_k be the number of ϵ measurements in the kth class and let $E_k(\mu_\Lambda, \sigma_\Lambda)$ be the expected number of measurements in that class under the assumption that our proposed model is true with lognormal parameters μ_Λ and σ_Λ. We then have

$$E_k(\mu_\Lambda, \sigma_\Lambda) = L \times (F_\epsilon(x_k) - F_\epsilon(x_{k-1})), \quad \text{(D6)}$$

which can be computed for a given μ_Λ and σ_Λ as outlined. We can then form the statistic

$$T(\mu_\Lambda, \sigma_\Lambda) = \sum_{k=1}^{K} \frac{(O_k - E_k(\mu_\Lambda, \sigma_\Lambda))^2}{E_k(\mu_\Lambda, \sigma_\Lambda)} = \sum_{k=1}^{K} \frac{O_k^2}{E_k(\mu_\Lambda, \sigma_\Lambda)} - L, \quad \text{(D7)}$$

where we have made use of the fact that

$$\sum_{k=1}^{K} O_k = \sum_{k=1}^{K} E_k(\mu_\Lambda, \sigma_\Lambda) = L. \quad \text{(D8)}$$

The minimum chi-square procedure is to estimate μ_Λ and σ_Λ as those values such that $T(\mu_\Lambda, \sigma_\Lambda)$ is minimized.

To find $\tilde{\mu}_\Lambda$ and $\tilde{\sigma}_\Lambda$ (here the tilde indicates a sample estimate), we must use a nonlinear optimization routine, for which it is helpful to have expressions for the partial derivatives of $T(\mu_\Lambda, \sigma_\Lambda)$ with respect to μ_Λ and σ_Λ. Here

$$\frac{\partial T(\mu_\Lambda, \sigma_\Lambda)}{\partial \mu_\Lambda} = -\sum_{k=1}^{K} \frac{O_k^2}{E_k^2(\mu_\Lambda, \sigma_\Lambda)} \frac{\partial E_k(\mu_\Lambda, \sigma_\Lambda)}{\partial \mu_\Lambda} = -\sum_{k=1}^{K} \frac{O_k^2}{E_k^2(\mu_\Lambda, \sigma_\Lambda)} \left(\frac{\partial F_\epsilon(x_k)}{\partial \mu_\Lambda} - \frac{\partial F_\epsilon(x_{k-1})}{\partial \mu_\Lambda}\right) = -\frac{1}{M} \sum_{k=1}^{K} \frac{O_k^2}{E_k^2(\mu_\Lambda, \sigma_\Lambda)} \sum_{j=1}^{M} \times \left(\frac{\partial F_\Lambda(x_k - n_j)}{\partial \mu_\Lambda} - \frac{\partial F_\Lambda(x_{k-1} - n_j)}{\partial \mu_\Lambda}\right). \quad \text{(D9)}$$

If $0 < x_k - n_j < \infty$, we have

$$\frac{\partial F_\Lambda(x_k - n_j)}{\partial \mu_\Lambda} = \frac{\partial \Phi\left(\dfrac{\ln(x_k - n_j) - \mu_\Lambda}{\sigma_\Lambda}\right)}{\partial \mu_\Lambda} = -\frac{1}{\sigma_\Lambda} \phi\left(\frac{\ln(x_k - n_j) - \mu_\Lambda}{\sigma_\Lambda}\right), \quad \text{where} \quad \phi(x) \equiv e^{-x^2/2}/\sqrt{2\pi}. \quad \text{(D10)}$$

On the other hand, if either $x_k \leq n_j$ or $x_k = \infty$, we have $\partial F_\Lambda(x_k - n_j)/\partial \mu_\Lambda = 0$. Likewise, we have

$$\frac{\partial T(\mu_\Lambda, \sigma_\Lambda)}{\partial \sigma_\Lambda} = -\frac{1}{M} \sum_{k=1}^{K} \frac{O_k^2}{E_k^2(\mu_\Lambda, \sigma_\Lambda)} \times \sum_{j=1}^{M} \left(\frac{\partial F_\Lambda(x_k - n_j)}{\partial \sigma_\Lambda} - \frac{\partial F_\Lambda(x_{k-1} - n_j)}{\partial \sigma_\Lambda}\right). \quad \text{(D11)}$$

If $0 < x_k - n_j < \infty$, we have

$$\frac{\partial F_\Lambda(x_k - n_j)}{\partial \sigma_\Lambda} = -\frac{\ln(x_k - n_j)}{\sigma_\Lambda^2} \phi\left(\frac{\ln(x_k - n_j) - \mu_\Lambda}{\sigma_\Lambda}\right); \quad \text{(D12)}$$

otherwise, we have $\partial F_\Lambda(x_k - n_j)/\partial \sigma_\Lambda = 0$.

Typical fits are shown in Fig. D1, and the resulting estimates for $\tilde{\mu}_\Lambda$ and $\tilde{\sigma}_\Lambda$ are shown in Fig. 7. The corresponding values for $T(\tilde{\mu}_\Lambda, \tilde{\sigma}_\Lambda)$ are given in Table D1.

If the ϵ_l's were independent of each other, we could assess whether the observed departures from the fitted

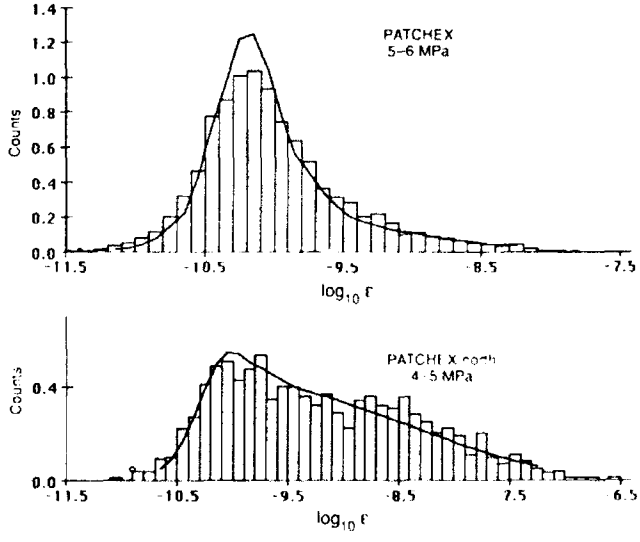

FIG. D1. Examples of χ^2 fits to histograms of observed 0.5-m $\log_{10}\epsilon$ taken in bins of 1 MPa.

TABLE D1. Chi-square statistics for fits to 0.5-m ϵ; L is the number of samples in each 1-MPa interval used for fitting, and K is the number of classes into which the observations were grouped (this number varies between 28 and 38 to ensure that each class contains at least 10 observations). If the L samples were independently distributed, the chi-square statistic $T(\tilde{\mu}_\Lambda, \tilde{\sigma}_\Lambda)$ would approximately follow a chi-square distribution with $K-3$ degrees of freedom (here $\tilde{\mu}_\Lambda$ and $\tilde{\sigma}_\Lambda$ are the minimum chi-square estimates of the lognormal parameters μ_Λ and σ_Λ). Because the samples are correlated, assessment of $T(\tilde{\mu}_\Lambda, \tilde{\sigma}_\Lambda)$ is problematic, but a Monte Carlo study of normally distributed band-limited white noise indicates that we have reasonable goodness of fit for PATCHEX north, whereas the opposite is true for PATCHEX.

	PATCHEX			PATCHEX north		
MPa	L	K	$T(\tilde{\mu}_\Lambda, \tilde{\sigma}_\Lambda)$	L	K	$T(\tilde{\mu}_\Lambda, \tilde{\sigma}_\Lambda)$
1–2	5361	38	332.1	993	36	78.4
2–3	5372	35	249.2	996	33	67.3
3–4	5382	32	326.8	997	33	107.9
4–5	5382	34	305.9	1000	37	53.0
5–6	5384	32	299.2	996	30	51.4
6–7	5396	29	292.5	998	38	80.8
7–8	5389	28	398.0	998	33	52.9
8–9	5393	30	316.1	997	36	48.9

distributions are consistent with random error by comparing the value of $T(\tilde{\mu}_\Lambda, \tilde{\sigma}_\Lambda)$ to a chi-square random variable with $K-3$ degrees of freedom (Conover 1980). Unfortunately, the ϵ_l are not anywhere close to being independent, but based on the assumption that correlation and distributional properties can be decoupled in a chi-square statistic, we can crudely determine the effect of different degrees of dependence on the chi-square statistic by the following procedure.

For an integer $M > 1$, consider a normally distributed band-limited white noise process with a low-frequency cutoff of $1/2M$. The theoretical autocovariance sequence for such noise is positive for lags less than M and is zero at lag M; hence, by choosing M in the range from 10 to 20, the autocovariance sequence for the band-limited process will mimic the observed sequence for the 0.5-m ϵ_l, which damps down to zero typically in the range from 5 to 10 m. We then generate samples from this process with a number of points comparable to those obtained in either PATCHEX (5380) or PATCHEX north (1000) and fit the data to a normal distribution using the minimum chi-square procedure outlined above. By replicating this procedure many different times and looking at the observed values of the chi-square statistic, we find that the range of observed chi-square statistics in the simulations matches very closely the range of values for $T(\tilde{\mu}_\Lambda, \tilde{\sigma}_\Lambda)$ shown in Table D1 for PATCHEX north. For PATCHEX, however, the values are about a factor of 2 to 3 larger than those in the simulation study. Thus, we conclude that our operational model fits the PATCHEX north data reasonably well, while there is evidence of a lack of fit in PATCHEX (this can be seen in Fig. D1, where the fitted distribution and the histogram disagree markedly in the central portion).

APPENDIX E

Theoretical q–q Plots

q–q plots of 10-m $\hat{\epsilon}$ and $\hat{\epsilon}_{iw}$

Let x_p be the pth quantile of the $\hat{\epsilon}_{iw}$ distribution. Then

$$p = \mathrm{P}[c\hat{S}^4_{10,l} \leq x_p] = \mathrm{P}[c\sigma_s^4 \chi^4_2 \leq x_p]$$
$$= \mathrm{P}[\chi^2_2 \leq \sqrt{x_p/c}/\sigma_s^2] = \mathrm{P}[\chi^2_2 \leq x'_p], \quad \text{(E1)}$$

where x'_p is the pth quantile of the χ^2_2 distribution. We thus have

$$x_p = (c\sigma^2 x'_p)^2. \quad \text{(E2)}$$

Next, let y_p be the pth quantile of the $\hat{\epsilon}$ distribution,

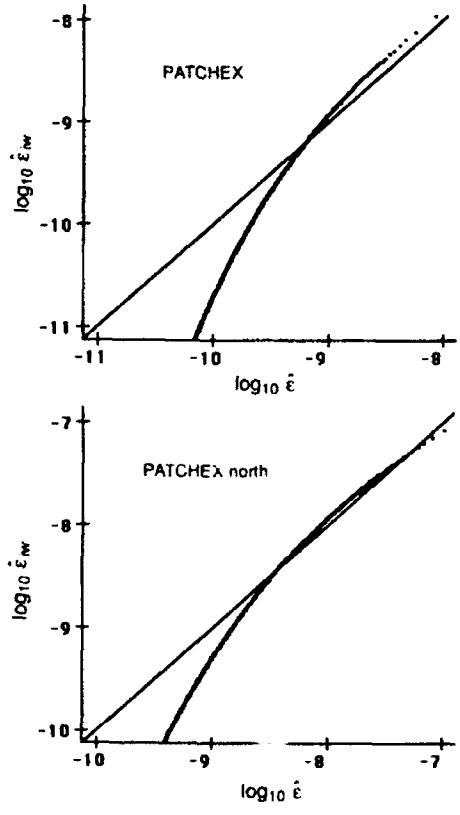

FIG. E1. Plots of theoretical q–q distributions for $\log_{10}\hat{\epsilon}_{iw}$ and $\log_{10}\hat{\epsilon}$ agree well at high magnitudes but not at low magnitudes

and let Z be a normal random variable with zero mean and unit variance; then

$$p = \mathrm{P}[\hat{\epsilon} \leqslant y_p] = \mathrm{P}\left[\frac{\log(\hat{\epsilon}) - \mu_{\ln\hat{\epsilon}}}{\sigma_{\ln\hat{\epsilon}}} \leqslant \frac{\log(y_p) - \mu_{\ln\hat{\epsilon}}}{\sigma_{\ln\hat{\epsilon}}}\right]$$

$$= \mathrm{P}\left[Z \leqslant \frac{\log(y_p) - \mu_{\ln\hat{\epsilon}}}{\sigma_{\ln\hat{\epsilon}}}\right] = \mathrm{P}[Z \leqslant y'_p], \qquad \text{(E3)}$$

where y'_p is the pth quantile of the standard normal distribution. We thus have

$$y_p = \exp(\mu_{\ln\hat{\epsilon}} + y'_p \sigma_{\ln\hat{\epsilon}}). \qquad \text{(E4)}$$

The q–q plots of these two theoretical distributions agree well at high magnitudes (Fig. E1).

APPENDIX F

Confidence Limits for $E(\hat{S}^2_{10})$ and $E(\hat{S}^4_{10})$

a. Confidence limits for $E(\hat{S}^2_{10})$

Previously we found that $\hat{S}^2_{10}$ is distributed as a rescaled χ^2 random variable with two degrees of freedom:

$$\frac{\hat{S}^2_{10,i}}{\sigma_s^2} = \frac{2\hat{S}^2_{10,i}}{E(\hat{S}^2_{10})} \overset{d}{=} \chi^2_2 \qquad \text{(F1)}$$

using $E(\hat{S}^2_{10}) = 2\sigma_s^2$. Averaging n of these $\hat{S}^2_{10,i}$ yields

$$\langle \hat{S}^2_{10} \rangle \equiv \frac{1}{n}\sum_{i=1}^{n} \hat{S}^2_{10,i} \overset{d}{=} \frac{E(\hat{S}^2_{10})}{2n}\chi^2_{2n} \qquad \text{(F2)}$$

or, equivalently,

$$\frac{2n\langle \hat{S}^2_{10} \rangle}{E(\hat{S}^2_{10})} \overset{d}{=} \chi^2_{2n}, \qquad \text{(F3)}$$

where χ^2_{2n} denotes a χ^2 random variable with $2n$ degrees of freedom.

To obtain confidence limits for $E(\hat{S}^2_{10})$, let $X^2_{2n,p}$ represent the $p \times 100$th percentage point of the χ^2 distribution with $2n$ degrees of freedom; that is,

$$\mathrm{P}[\chi^2_{2n} \leqslant X^2_{2n,p}] = p, \qquad \text{(F4)}$$

where $\mathrm{P}[A]$ refers to the probability of the event A. Then

$$\mathrm{P}[X^2_{2n,(1-p)/2} \leqslant \frac{2n\langle \hat{S}^2_{10} \rangle}{E(\hat{S}^2_{10})} \leqslant X^2_{2n,(1+p)/2}] = p. \qquad \text{(F5)}$$

This is equivalent to

$$\mathrm{P}\left[\frac{2n\langle \hat{S}^2_{10} \rangle}{X^2_{2n,(1+p)/2}} \leqslant E(\hat{S}^2_{10}) \leqslant \frac{2n\langle \hat{S}^2_{10} \rangle}{X^2_{2n,(1-p)/2}}\right] = p. \qquad \text{(F6)}$$

Therefore, the $p \times 100\%$ confidence interval for $E(\hat{S}^2_{10})$ is

$$[L_n \times \langle \hat{S}^2_{10} \rangle,\ U_n \times \langle \hat{S}^2_{10} \rangle], \qquad \text{(F7)}$$

where

$$L_n \equiv \frac{2n}{X^2_{2n,(1+p)/2}} \quad \text{and} \quad U_n \equiv \frac{2n}{X^2_{2n,(1-p)/2}}. \qquad \text{(F8)}$$

To evaluate $X^2_{2n,p}$, we use Eq. (3) of Zar (1978); to input x, the standardized normal deviate, we use the approximation for $\Phi^{-1}(p)$ in Table 6.5 of Chambers et al. (1983).

b. Confidence limits for $E(\hat{S}^4_{10})$

As noted in the main text, confidence limits for $E(\hat{S}^4_{10})$ can be based either on $\langle \hat{S}^2_{10} \rangle$ or on

$$\langle \hat{S}^4_{10} \rangle \equiv \frac{1}{n}\sum_{i=1}^{n} \hat{S}^4_{10,i}. \qquad \text{(F9)}$$

Let Q_n denote the average of the squares of n independently distributed χ^2_2 random variables, and let $Q_{n,p}$ represent the $p \times 100$th percentage point of the distribution of Q_n; that is, $\mathrm{P}[Q_n \leqslant Q_{n,p}] = p$. A $p \times 100\%$ confidence interval for $E(\hat{S}^4_{10})$ is given by

$$[L'_n \times \langle \hat{S}^4_{10} \rangle,\ U'_n \times \langle \hat{S}^4_{10} \rangle], \qquad \text{(F10)}$$

where

$$L'_n = \frac{8}{Q_{n,(1+p)/2}} \quad \text{and} \quad U'_n = \frac{8}{Q_{n,(1-p)/2}}. \qquad \text{(F11)}$$

The percentage points $Q_{n,p}$ can be determined either by Monte Carlo simulations or, if $n \geqslant 100$, by an Edgeworth approximation to the distribution of Q_n [see section 1.5.D of Bickel and Doksum (1977)].

APPENDIX G

Comments on Baker and Gibson (1987)

Baker and Gibson (1987) urge using lognormal statistics to estimate $\langle \epsilon \rangle$ in the thermocline. We agree that lognormal statistics are useful for planning field measurements, but do not concur that they should be routine for post facto data analysis. In the first place, not all datasets are lognormal. As noted in the text, our ϵ profiles are definitely not lognormal unless scaled with $\langle N^2 \rangle$ and corrected for noise. Second, at present there is no rigorous model demonstrating under what conditions ϵ should be lognormal in the thermocline. Our hypothesis in this paper is that lognormality of scaled and noise-corrected data is an approximate rather than an exact condition.

Third, Baker and Gibson (1987) claim that the mle-based estimator $\bar{X}_{\mathrm{mle}}$ of the parameter μ has smaller

TABLE G1. Statistics of 10-m dissipation between 1 and 9 MPa. For small samples of lognormal distributions, arithmetic estimators of the mean are more efficient than maximum likelihood estimators; that is, $\mathrm{var}\{\bar{X}_{\mathrm{am}}\} < \mathrm{var}\{\bar{X}_{\mathrm{mle}}\}$ for $n \leq 21$. For $n < 10$ the efficiency is infinite.

n	$\mathrm{var}\{\bar{X}_{\mathrm{mle}}\}$	$\mathrm{var}\{\bar{X}_{\mathrm{am}}\}$	Ratio (efficiency)
10	41 381 397 761	259 156	159 678
15	631 252	172 771	3.65
20	153 173	129 578	1.18
21	128 300	123 408	1.04
22	109 528	117 798	0.93
25	74 122	103 662	0.71
50	16 761	51 831	0.32
100	6 046	25 916	0.23
∞	—	—	0.17

variance than the sample mean $\bar{X}_{\mathrm{am}}$. This is true for moderate-to-large sample sizes, but it is *not* true for very small samples. In fact, for samples sizes n such that

$$n \leq 2\sigma^2 + 1 \qquad \text{(G1)}$$

the variance of $\bar{X}_{\mathrm{mle}}$ is infinite! This condition is correctly stated by Baker and Gibson following their Eq. (B11), but they do not note its practical implications. This becomes an issue in their section 3, where they represent an example from Gregg (1977) with $\sigma^2 = 4.41$ and $n = 10$. For this value of σ^2, $n = 10$ is the smallest sample size for which $\mathrm{var}\{\bar{X}_{\mathrm{mle}}\}$ is finite. If we use their Eqs. (B10) and (B11), we can compute $\mathrm{var}\{\bar{X}_{\mathrm{mle}}\}$, $\mathrm{var}\{\bar{X}_{\mathrm{am}}\}$ and their ratio for small n. Table G1 shows that, for $n \leq 21$, we should prefer $\bar{X}_{\mathrm{am}}$ over $\bar{X}_{\mathrm{mle}}$ as our estimator of μ, while the opposite holds for $n > 21$. (Note that their Fig. B1 only shows the relative efficiency for moderate n, namely, 50 and 100.)

If we are dealing with correlated data rather than uncorrelated data as Baker and Gibson assume, the minimum sample size for which $\bar{X}_{\mathrm{mle}}$ is preferable over $\bar{X}_{\mathrm{am}}$ will certainly be larger.

It should also be noted that confidence intervals based on mle's are not necessarily valid when other estimates are used. Thus, Baker and Gibson's claim that mle-based confidence intervals can be used with their graphical estimates is not correct. To be specific, the claim that their equation (7) still holds when 1) the graphical estimator is used and 2) there is substantial noise cannot be supported by appealing to the noiseless case (as the authors do in their discussion of Fig. 4b). As can be seen from a limiting case argument (i.e., all noise), there *must* be some dependence on the number of points included in the graphical fit, but they claim there is none. Furthermore, their graphical estimates of $\tilde{\mu}_{\ln}$ and $\tilde{\sigma}_{\ln}$ are not maximum likelihood estimates.

REFERENCES

Baker, M. A., and C. H. Gibson, 1987: Sampling turbulence in the stratified ocean: Statistical consequences of strong intermittency. *J. Phys. Oceanogr.*, **17**, 1817–1836.

Bartlett, M. S., and D. G. Kendall, 1946: The statistical analysis of variance-heterogeneity and the logarithmic transformation. *J. Roy. Stat. Soc. Suppl.*, **7**, 128–133.

Bendat, J. S., and A. G. Piersol, 1971: *Random Data: Analysis and Measurement Procedures*. Wiley-Interscience, 407 pp.

Bickel, P. J., and K. A. Doksum, 1977: *Mathematical Statistics: Basic Ideas and Selected Topics*. Holden-Day, 493 pp.

Briscoe, M. G., and R. A. Weller, 1984: Preliminary results from the long-term upper-ocean study (LOTUS). *Dyn. Atmos. Oceans*, **8**, 243–265.

Cairns, J. L., and G. O. Williams, 1976: Internal wave observations from a midwater float, 2. *J. Geophys. Res.*, **81**, 1943–1950.

Chambers, J. M., W. S. Cleveland, B. Kleiner, and P. A. Tukey, 1983: *Graphical Methods for Data Analysis*. Duxbury Press, 395 pp.

Conover, W. J., 1980: *Practical Nonparametric Statistics*, 2d ed. Wiley, 493 pp.

D'Asaro, E. A., and H. Perkins, 1984: A near-inertial internal wave spectrum for the Sargasso Sea in late summer. *J. Phys. Oceanogr.*, **14**, 489–505.

Desaubies, Y., and W. K. Smith, 1982: Statistics of Richardson number and instability in oceanic internal waves. *J. Phys. Oceanogr.*, **12**, 1245–1259.

Eriksen, C. C., 1978: Measurements and models of fine structure, internal gravity waves, and wave breaking in the deep ocean. *J. Geophys. Res.*, **83**, 2989–3009.

——, 1982: Observations of internal wave reflections off sloping bottoms. *J. Geophys. Res.*, **87**, 525–538.

Gargett, A. E., 1990: Do we really know how to scale the turbulent kinetic energy dissipation rate ϵ due to breaking of oceanic internal waves? *J. Geophys. Res.*, **95**, 15 971–15 974.

Garrett, C. J. R., and W. H. Munk, 1972a: Space-time scales of internal waves. *Geophys. Fluid Dyn.*, **3**, 225–264.

——, and ——, 1972b: Oceanic mixing by breaking internal waves. *Deep-Sea Res.*, **19**, 823–832.

——, and ——, 1975: Space-time scales of internal waves: A progress report. *J. Geophys. Res.*, **80**, 291–297.

Gibson, C. H., 1981: Buoyancy effects in turbulent mixing: sampling turbulence in the stratified ocean. *Amer. Inst. Aeronaut. Astronaut. J.*, **19**, 1394–1400.

Gregg, M. C., 1977: Variations in the intensity of small-scale mixing in the main thermocline. *J. Phys. Oceanogr.*, **7**, 436–454.

——, 1980: Microstructure patches in the thermocline. *J. Phys. Oceanogr.*, **10**, 915–943.

——, 1989: Scaling turbulent dissipation in the thermocline. *J. Geophys. Res.*, **94**, 9686–9698.

——, and T. B. Sanford, 1988: The dependence of turbulent dissipation on stratification in a diffusively stable thermocline. *J. Geophys. Res.*, **93**, 12 381–12 392.

——, E. A. D'Asaro, T. J. Shay, and N. Larson, 1986: Observations of persistent mixing and near-inertial internal waves. *J. Phys. Oceanogr.*, **16**, 856–885.

——, D. P. Winkel, and T. B. Sanford, 1992: Varieties of fully resolved spectra of vertical shear. *J. Phys. Oceanogr.*, **23**, 124–141.

Gurvich, A. S., and A. M. Yaglom, 1967: Breakdown of eddies and probability distributions for small-scale turbulence. *Phys. Fluids*, **10**(Suppl.), S59–S65.

Henyey, F. S., J. Wright, and S. M. Flatté, 1986: Energy and action flow through the internal wave field: An eikonal approach. *J. Geophys. Res.*, **91**, 8487–8495.

Jenkins, G. M., and D. G. Watts, 1969: *Spectral Analysis and Its Applications*. Holden-Day, 525 pp.

Land, C. E., 1972: An evaluation of approximate confidence interval estimation methods for lognormal means. *Technometrics*, **14**, 145–158.

——, 1975: Tables of confidence limits for linear functions of the normal mean and variance. *Selected Tables in Mathematical Statistics*, III, H. L. Harter and D. B. Owen, Eds., Amer. Math. Soc., 385–419.

Mason, A. L., and C. B. Bell, 1986: New Lilliefors and Srinivasan table with applications. *Commun. Statist.–Simula.*, **15**, 451–477.

McComas, C. H., and P. Müller, 1981: The dynamic balance of internal waves. *J. Phys. Oceanogr.*, **11**, 970–986.

Miles, J. W., 1961: On the stability of heterogeneous shear flows. *J. Fluid Mech.*, **16**, 207–227.

Munk, W. H., 1981: Internal waves and small-scale processes. *Evolution of Physical Oceanography, Scientific Surveys in Honor of Henry Stommel*, B. A. Warren and C. Wunsch, Eds., The MIT Press, 264–291.

Osborn, T. R., and W. R. Crawford, 1980: An airfoil probe for measuring turbulent velocity fluctuations in water. *Air-Sea Interactions: Instruments and Methods*, F. Dobson, L. Hasse, and R. Davis, Eds., 369–386.

Papoulis, A., 1984: *Probability, Random Variables, and Stochastic Processes*, 2d ed., McGraw-Hill, 576 pp.

Press, W. H., B. P. Flannery, S. A. Teukolsky, and W. T. Vetterling, 1988: *Numerical Recipes in C: The Art of Scientific Computing*, Cambridge University Press, 735 pp.

Priestley, M. B., 1981: *Spectral Analysis and Time Series*, Academic Press, 890 pp.

Smart, J. H., 1988: Comparison of modelled and observed dependence of shear on stratification in the upper ocean. *Dyn. Atmos. Oceans*, **12**, 127–142.

Stephens, M. A., 1974: EDF statistics for goodness of fit and some comparisons. *J. Statist. Soc. Amer.*, **69**, 730–737.

Washburn, R. B., and C. H. Gibson, 1984: Horizontal variability of temperature microstructure at the base of a mixed layer during MILE. *J. Geophys. Res.*, **89**, 3507–3522.

Yamazaki, H., and R. Lueck, 1990: Why oceanic dissipation rates are not lognormal. *J. Phys. Oceanogr.*, **20**, 1907–1918.

Zar, J. H., 1978: Approximations for the percentage points of the chi-squared distribution. *Appl. Statist.*, **27**, 280–290.